
BAYESIAN JOINT ADDITIVE FACTOR MODELS FOR MULTIVIEW LEARNING

Niccolo Anceschi

Department of Statistical Science
Duke University
Durham, NC 27708, USA
niccolo.anceschi@duke.edu

Federico Ferrari

Biostatistics and Research Decision Sciences
Merck & Co., Inc.
Rahway, NJ 07065, USA
federico.ferrari@merck.com

David B. Dunson*

Department of Statistical Science
Duke University
Durham, NC 27708, USA
dunson@duke.edu

Himel Mallick*

Division of Biostatistics, Department of Population Health Sciences
Weill Cornell Medicine, Cornell University
New York, NY 10065, USA
him4004@med.cornell.edu

ABSTRACT

It is increasingly common in a wide variety of applied settings to collect data of multiple different types on the same set of samples. Our particular focus in this article is on studying relationships between such multiview features and responses. A motivating application arises in the context of precision medicine where multi-omics data are collected to correlate with clinical outcomes. It is of interest to infer dependence within and across views while combining multimodal information to improve the prediction of outcomes. The signal-to-noise ratio can vary substantially across views, motivating more nuanced statistical tools beyond standard late and early fusion. This challenge comes with the need to preserve interpretability, select features, and obtain accurate uncertainty quantification. We propose a joint additive factor regression model (JAFAR) with a structured additive design, accounting for shared and view-specific components. We ensure identifiability via a novel dependent cumulative shrinkage process (D-CUSP) prior. We provide an efficient implementation via a partially collapsed Gibbs sampler and extend our approach to allow flexible feature and outcome distributions. Prediction of time-to-labor onset from immunome, metabolome, and proteome data illustrates performance gains against state-of-the-art competitors. Our open-source software (R package) is available at <https://github.com/niccoloanceschi/jafar>.

Keywords Bayesian inference · Multiview data integration · Factor analysis · Identifiability · Latent variables · Precision medicine

1 Introduction

In personalized medicine, it is common to gather vastly different kinds of complementary biological data by simultaneously measuring multiple assays in the same subjects, ranging across the genome, epigenome, transcriptome, proteome, and metabolome (Stelzer et al. 2021, Ding et al. 2022). Integrative analyses

*Co-corresponding authors

that combine information across such data views can deliver more comprehensive insights into patient heterogeneity and the underlying pathways dictating health outcomes (Mallick et al. 2024). Similar setups arise in diverse scientific contexts including wearable devices, electronic health records, and finance, among others (Lee & Yoo 2020, Li et al. 2021, McNaboe et al. 2022), where there is enormous potential to integrate the concurrent information from distinct vantage points to better understand between-view associations and improve prediction of outcomes.

Multiview datasets have specific characteristics that complicate their analyses: (i) they are often high-dimensional, noisy, and heterogeneous, with confounding effects unique to each layer (e.g., platform-specific batch effects); (ii) sample sizes are often very limited, particularly in clinical applications; and (iii) signal-to-noise ratios can vary substantially across views, which must be accounted for in the analysis to avoid poor results. Many methods face difficulties in identifying the predictive signal since it is common for most of the variability in the multiview features to be unrelated to the response (Carvalho et al. 2008). Our primary motivation in this article is thus to enable accurate and interpretable outcome prediction while allowing inferences on within- and across-view dependence structures. By selecting important latent variables within and across views, we aim to improve interpretability and reduce the burden of future data collection efforts by focusing measurements on response-relevant variables.

Carefully structured factor models that infer low-dimensional joint- and view-specific sources of variation are particularly promising. Early contributions in this space focused on the unsupervised paradigm (Lock et al. 2013, Li & Jung 2017, Argelaguet et al. 2018). Two-step approaches exploiting the learned factorization often fail to identify subtle response-relevant factors, leading to subpar predictive accuracy (Samorodnitsky et al. 2024). More recent contributions considered integrative factorizations in a supervised setting (Palzer et al. 2022, Li & Li 2022, Samorodnitsky et al. 2024). Among these, Bayesian Simultaneous Factorization and Prediction (BSFP) uses an additive factor regression structure in which the response loads on shared- and view-specific factors (Samorodnitsky et al. 2024). Although BSFP considers a dependence-aware formulation, it does not address the crucial identifiability issue that can harm interpretability, stability, and predictive accuracy. Alternative approaches focusing on prediction accuracy include Cooperative Learning (Ding et al. 2022) and IntegratedLearner (Mallick et al. 2024). Both these methods combine the usual squared-error loss-based predictions with a suitable machine learning algorithm. However, by conditioning on the multiview features, neither approach allows inferences on or exploits information from inter- and intra-view correlations. One typical consequence of this is a tendency for unstable and unreliable feature selection, as from a predictive standpoint, it is sufficient to select any one of a highly correlated set of features.

To address these gaps, we propose a joint additive factor regression approach, JAFAR (Joint Additive Factor Regression). Instead of allowing the responses to load on all factors, JAFAR generalizes the approach of Moran et al. (2021) to the multiview case, isolating sources of variation into shared and view-specific components. This, in turn, facilitates the identification of response-relevant latent factors, while also leading to computational and mixing improvements. We use a partially collapsed Gibbs sampler (Park & van Dyk 2009) that benefits from the marginalization of the view-specific factors. We ensure the identifiability of the additive components of the factor model by extending the cumulative shrinkage process prior (CUSP) (Legramanti et al. 2020) to introduce dependence among the shared-component loadings for different views. In addition, we propose a modification of the `Varimax` step in `MatchAlign` (Poworoznek et al. 2021) to preserve the composite structure in the shared loadings when solving rotational ambiguity. JAFAR is validated using both simulation studies and real data analysis where it outperforms published methods in estimation and prediction.

The remainder of the paper is organized as follows. The proposed methodology is presented in detail in Section 2, including an initial Gaussian specification and flexible semiparametric extensions. In Section 3, we focus on simulation studies to validate the performances of JAFAR against state-of-the-art competitors. The empirical studies from Section 4 further showcase the benefits of our contribution on real data. An open-source implementation of JAFAR is available through R package `jafar`.

2 Multiview Factor Analysis

To better highlight the nuances of our additive factor regression model, we first describe the related BSFP construction (Samorodnitsky et al. 2024), which takes the following form:

$$\begin{aligned} \mathbf{x}_{mi} &= \mathbf{\Lambda}_m \boldsymbol{\eta}_i + \mathbf{\Gamma}_m \boldsymbol{\phi}_{mi} + \boldsymbol{\epsilon}_{mi} \\ y_i &= \mu_y + \boldsymbol{\theta}_0^\top \boldsymbol{\eta}_i + \sum_{m=1}^M \boldsymbol{\theta}_m^\top \boldsymbol{\phi}_{mi} + e_i, \end{aligned} \quad (1)$$

where $\mathbf{x}_{mi} \in \mathbb{R}^{p_m}$ and $y_i \in \mathbb{R}$ represent the multiview data and the response, respectively, for each statistical unit $i \in \{1, \dots, n\}$ and modality $m \in \{1, \dots, M\}$. Here, $\mathbf{\Lambda}_m \in \mathbb{R}^{p_m \times K_m}$ and $\mathbf{\Gamma}_m \in \mathbb{R}^{p_m \times K}$ are loadings matrices associated with shared and view-specific latent factors, $\boldsymbol{\eta}_i \in \mathbb{R}^{n \times K}$ and $\boldsymbol{\phi}_{mi} \in \mathbb{R}^{n \times K_m}$, respectively. In BSFP, the response is allowed to load on all latent factors via the set of factor regression coefficients $\boldsymbol{\theta}_0 \in \mathbb{R}^K$ and $\boldsymbol{\theta}_m \in \mathbb{R}^{K_m}$, complemented with an offset term $\mu_y \in \mathbb{R}$. The residual components e_i and $\boldsymbol{\epsilon}_{mi}$ are assumed to follow normal distributions $\mathcal{N}(0, \sigma_y^2)$ and $\mathcal{N}_{p_m}(\mathbf{0}_{p_m}, \text{diag}(\boldsymbol{\sigma}_m^2))$, with $\boldsymbol{\sigma}_m^2 = \{\sigma_{mj}^2\}_{j=1}^{p_m}$. Samorodnitsky et al. (2024) set $\sigma_y^2 = 1$ and $\sigma_{mj}^2 = 1$ for all $j = 1, \dots, p_m$, after rescaling the data to have unit error variance rather than unit overall variance. This is achieved via the median absolute deviation estimator of standard deviation in Gavish & Donoho (2017). For the prior and latent variable distributions, the authors choose

$$\begin{aligned} \boldsymbol{\eta}_i &\sim \mathcal{N}_K(\mathbf{0}_K, r_o^2 \mathbf{I}_K) & \mathbf{\Lambda}_{mj} &\sim \mathcal{N}_K(\mathbf{0}_K, r_o^2 \mathbf{I}_K) \\ \boldsymbol{\phi}_{mi} &\sim \mathcal{N}_{K_m}(\mathbf{0}_{K_m}, r_m^2 \mathbf{I}_{K_m}) & \mathbf{\Gamma}_{mj} &\sim \mathcal{N}_K(\mathbf{0}_K, r_m^2 \mathbf{I}_K), \end{aligned} \quad (2)$$

further assuming conditionally conjugate priors on $\mu_y, \boldsymbol{\theta}_0, \boldsymbol{\theta}_m, \sigma_y^2$, and $\boldsymbol{\sigma}_m^2$. This is mostly for computational convenience, as posterior inference can proceed via Gibbs sampling.

To both speed up the exploration phase of Markov chain Monte Carlo (MCMC) and fix the numbers of latent factors, the authors initialize the Gibbs Sampler at the solution over $\boldsymbol{\eta}$ and $\{\boldsymbol{\phi}_m, \mathbf{\Lambda}_m, \mathbf{\Gamma}_m\}_{m=1}^M$ of the optimization problem (UNIFAC)

$$\begin{aligned} \min \left\{ \sum_{m=1}^M \|\mathbf{X}_m - \boldsymbol{\eta} \mathbf{\Lambda}_m^\top - \boldsymbol{\phi}_m \mathbf{\Gamma}_m^\top\|_F^2 + r_o^{-2} \|\boldsymbol{\eta}\|_F^2 + \sum_{m=1}^M r_o^{-2} \|\mathbf{\Lambda}_m\|_F^2 \right. \\ \left. + \sum_{m=1}^M r_m^{-2} \|\boldsymbol{\phi}_m\|_F^2 + \sum_{m=1}^M r_m^{-2} \|\mathbf{\Gamma}_m\|_F^2 \right\}. \end{aligned}$$

This corresponds to the maximum a posteriori equation for the marginal model on the features without the response. Let $\boldsymbol{\eta} = [\boldsymbol{\eta}_1^\top, \dots, \boldsymbol{\eta}_n^\top]^\top \in \mathbb{R}^{n \times K}$, $\boldsymbol{\phi}_m = [\boldsymbol{\phi}_{m1}^\top, \dots, \boldsymbol{\phi}_{mn}^\top]^\top \in \mathbb{R}^{n \times K_m}$, and $\mathbf{X}_m = [\mathbf{x}_{m1}^\top, \dots, \mathbf{x}_{mn}^\top]^\top \in \mathbb{R}^{n \times p_m}$, with $\|\cdot\|_F$ the Frobenius norm. The penalty can be equivalently represented in terms of nuclear norms of $\boldsymbol{\phi}_m \mathbf{\Gamma}_m^\top$ and $\boldsymbol{\eta} [\mathbf{\Lambda}_1^\top, \dots, \mathbf{\Lambda}_M^\top]$, which is the sum of singular values. The minimum is achieved via an iterative soft singular value thresholding algorithm, that retains singular values greater than r_m^{-2} and r_o^{-2} respectively. This performs rank selection for both shared and view-specific components, i.e. determining the values of K and K_m . The authors set $r_o^{-2} = \sqrt{n} + \sqrt{\sum_m p_m}$ and $r_m^{-2} = \sqrt{n} + \sqrt{p_m}$, motivated by theoretical arguments on the residual information not captured by the low-rank decomposition.

The simple structure of BSFP comes at the expense of several shortcomings. Non-identifiability of shared versus specific factors in additive factor models is not addressed (Chandra, Dunson & Xu 2023). Shared factors have more descriptive power than view-specific ones (refer to Section 2.1). Unless constrained otherwise, the tendency is to use some columns of $\boldsymbol{\eta}$ to explain sources of variation related to a single view; in our experience, this often occurs even under the UNIFAC initialization for K . This hinders MCMC mixing and interpretability of the inferred sources of variation. Furthermore, the simple prior structure on the loadings matrices makes the model prone to severe covariance underestimation in high-dimensional scenarios.

A rich literature on Bayesian factor models has developed structured shrinkage priors for the loading matrices (Bhattacharya & Dunson 2011, Bhattacharya et al. 2015, Legramanti et al. 2020, Schiavon et al. 2022), in an effort to capture meaningful latent sources of variability in high dimensions. Simply plugging in such priors within the BSFP construction can lead to unsatisfactory prediction of low-dimensional health-related outcomes. There is a tendency for the inferred latent factors to be dominated by the high-dimensional

features with very weak supervision by the low-dimensional outcome (Hahn et al. 2013). This needs to be carefully dealt with to avoid low predictive accuracy, as shown in the empirical studies from Section 4.

2.1 Joint Additive Factor Regression (JAFAR)

To address all the aforementioned issues and deliver accurate response prediction from multiview data, we propose employing the following joint additive factor regression model

$$\begin{aligned}\mathbf{x}_{mi} &= \boldsymbol{\mu}_m + \boldsymbol{\Lambda}_m \boldsymbol{\eta}_i + \boldsymbol{\Gamma}_m \boldsymbol{\phi}_{mi} + \boldsymbol{\epsilon}_{mi} \\ y_i &= \mu_y + \boldsymbol{\theta}^\top \boldsymbol{\eta}_i + e_i.\end{aligned}\quad (3)$$

The proposed structure is similar to BSFP, but with important structural differences. Analogously to Moran et al. (2021), the local factors $\{\boldsymbol{\phi}_{mi}\}_{m=1}^M$ only capture view-specific variability unrelated to the response. The shared factors $\boldsymbol{\eta}_i$ impact at least two data components, either two covariate views or one view and the response. This restriction is key to identifiability and leads to much-improved mixing. Below we provide additional details on identifiability and then describe a carefully structured prior for the loadings in our model.

2.1.1 Non-identifiability of additive factor models

Identifiability of the local versus global components of the model is of substantial practical importance. There is a parallel literature on multi-study factor models that also have local and global components (Vito et al. 2021); in this context, the benefits of imposing identifiability have been clearly shown (Chandra, Dunson & Xu 2023). To illustrate non-identifiability, we first express JAFAR in terms of a unique set of loadings matrices $\tilde{\boldsymbol{\Lambda}}_m$, shared factors $\tilde{\boldsymbol{\eta}}_i$ and regression coefficients $\tilde{\boldsymbol{\theta}}$:

$$\begin{aligned}\tilde{\boldsymbol{\Lambda}}_m &= [\boldsymbol{\Lambda}_m, \mathbf{0}_{p_m \times K_1}, \dots, \mathbf{0}_{p_m \times K_{m-1}}, \boldsymbol{\Gamma}_m, \mathbf{0}_{p_m \times K_{m+1}}, \dots, \mathbf{0}_{p_m \times K_M}] \\ \tilde{\boldsymbol{\eta}}_i &= [\boldsymbol{\eta}_i, \boldsymbol{\phi}_{1i}, \dots, \boldsymbol{\phi}_{Mi}] \quad \tilde{\boldsymbol{\theta}} = [\boldsymbol{\theta}^\top, \mathbf{0}_{K_1}^\top, \dots, \mathbf{0}_{K_M}^\top]^\top,\end{aligned}\quad (4)$$

while dropping all view-specific components. BSFP has an equivalent representation except with $\tilde{\boldsymbol{\theta}} = [\boldsymbol{\theta}_0^\top, \boldsymbol{\theta}_1^\top, \dots, \boldsymbol{\theta}_M^\top]^\top$. This shows an equivalence between additive local-global factor models and global-only factor models with an appropriate sparsity pattern in the loadings. Marginalizing out latent factors, the induced inter- and intra-view covariances are:

$$\text{cov}(\mathbf{x}_m) = r_o \boldsymbol{\Lambda}_m \boldsymbol{\Lambda}_m^\top + r_m \boldsymbol{\Gamma}_m \boldsymbol{\Gamma}_m^\top + \text{diag}(\boldsymbol{\sigma}_m^2), \quad \text{cov}(\mathbf{x}_m, \mathbf{x}_{m'}) = r_o \boldsymbol{\Lambda}_m \boldsymbol{\Lambda}_{m'}^\top. \quad (5)$$

The factor's prior variances are $r_o = r_m = 1$ for JAFAR and $r_o = 1/(\sqrt{n} + \sqrt{\sum_m p_m})$, $r_m = 1/(\sqrt{n} + \sqrt{\sum_m p_m})$ for BSFP. Concatenating all views into $\mathbf{x} = [\mathbf{x}_1^\top, \dots, \mathbf{x}_M^\top]^\top$, this entails that the view-specific components $\boldsymbol{\Gamma}_m$ affect only the block-diagonal element of the induced covariance. Hence, dropping the shared loadings $\boldsymbol{\Lambda}_m$ from the model forces zero across-view correlation.

Recent contributions in the literature addressed the analogous issues in multi-study additive factor models via different structural modifications of the original modeling formulation (Roy et al. 2021, Chandra, Dunson & Xu 2023). Here we take a different approach, achieving identifiability via a suitable prior structure for the loadings of the shared component in equation (3).

2.2 Prior formulation

To maintain computational tractability in high dimensions, we assume conditionally conjugate priors for most components of the model.

$$\begin{aligned}\boldsymbol{\eta}_i &\stackrel{\text{iid}}{\sim} \mathcal{N}_K(\mathbf{0}_K, \mathbf{I}_K) & \mu_y &\stackrel{\text{iid}}{\sim} \mathcal{N}(0, v_y^2) & \sigma_y^2 &\stackrel{\text{iid}}{\sim} \text{InvG}a(a^{(y)}, b^{(y)}) \\ \boldsymbol{\phi}_{mi} &\stackrel{\text{iid}}{\sim} \mathcal{N}_{K_m}(\mathbf{0}_{K_m}, \mathbf{I}_{K_m}) & \mu_{mj} &\stackrel{\text{iid}}{\sim} \mathcal{N}(0, v_m^2) & \sigma_{mj}^2 &\stackrel{\text{iid}}{\sim} \text{InvG}a(a^{(m)}, b^{(m)})\end{aligned}$$

We assume independent standard normal priors for all factors, consistently with standard practice. To impose identifiability, we propose an extension of the CUSP prior of Legramanti et al. (2020). CUSP adaptively

removes unnecessary factors from an over-fitted factor model by progressively shrinking the loadings to zero. This is achieved by leveraging stick-breaking representations of Dirichlet processes (Ishwaran & James 2001). We assume independent CUSP priors for the view-specific loadings $\mathbf{\Gamma}_m \sim \text{CUSP}(a_m^{(r)}, b_m^{(r)}, \tau_{m\infty}^2, \alpha_m^{(r)})$, with

$$\mathbf{\Gamma}_{mjh} \sim \mathcal{N}(0, \tau_{mh}^2) \quad \tau_{mh}^2 \sim \pi_{mh} \text{InvGa}(a_m^{(r)}, b_m^{(r)}) + (1 - \pi_{mh}) \delta_{\tau_{m\infty}^2}.$$

Accordingly, the increasing shrinkage behavior is induced by the weight of the spike and slab

$$\pi_{mh} = 1 - \sum_{l=1}^h \omega_{ml} \quad \omega_{mh} = \nu_{mh} \prod_{l=1}^{h-1} (1 - \nu_{ml}) \quad \nu_{mh} \sim \mathcal{B}e(1, \alpha_m^{(r)}),$$

such that $\mathbb{P}[|\mathbf{\Gamma}_{mjh+1}| \leq \varepsilon] > \mathbb{P}[|\mathbf{\Gamma}_{mjh}| \leq \varepsilon] \forall \varepsilon > 0$, provided that $b_m^{(r)}/a_m^{(r)} > \tau_{m\infty}^2$. The stick-breaking process can be rewritten in terms of discrete latent indicators $\zeta_{mh} \in \mathbb{N}$, where a priori $\mathbb{P}[\zeta_{mh} = l] = \omega_{ml}$ for each $h, l \geq 1$, such that $\pi_{mh} = \mathbb{P}[\zeta_{mh} > h]$. The h^{th} column is defined as active when it is sampled from the slab, namely if $\zeta_{mh} > h$, and inactive otherwise. It is standard practice to truncate the number of factors to conservative upper bounds K_m . This retains sufficient flexibility while allowing for tractable posterior inference via a conditionally conjugate Gibbs sampler. The upper bounds can be tuned as part of the inferential procedure via an adaptive Gibbs sampler. This amounts to dropping the inactive columns of Λ_m while preserving a buffer inactive factor in the rightmost column, provided that suitable diminishing adaptation conditions are satisfied (Roberts & Rosenthal 2007).

2.2.1 Dependent cumulative shrinkage processes (D-CUSP)

We tackle non-identifiability between shared and view-specific factors via a novel joint prior structure for the shared loading matrices $\{\Lambda_m\}_{m=1}^M$ and factor regression coefficients θ . We place zero prior mass on configurations where any shared factor is active in less than two model components. Similar to the spike and slab structure in the original CUSP formulation, we let

$$\begin{aligned} \Lambda_{mjh} &\sim \mathcal{N}(0, \chi_{mh}^2) & \chi_{mh}^2 &\sim \psi_{mh} \text{InvGa}(a_m^{(\Lambda)}, b_m^{(\Lambda)}) + (1 - \psi_{mh}) \delta_{\chi_{m\infty}^2} \\ \theta_h &\sim \mathcal{N}(0, \chi_h^2) & \chi_h^2 &\sim \psi_h \text{InvGa}(a^{(\theta)}, b^{(\theta)}) + (1 - \psi_h) \delta_{\chi_{\infty}^2}, \end{aligned}$$

where now we introduce dependence across the views and response via the spike and slab mixture weights ψ_h and $\{\psi_{mh}\}_{m=1}^M$. This can be done by leveraging the representation in terms of latent indicator variables $\{\{\delta_{mh}\}_{h \geq 1}\}_{m=1}^M$ and $\{\delta_h\}_{h \geq 1}$, where $\delta_{mh} \in \mathbb{N}$ and $\delta_h \in \{0, 1\}$. As before, each column of the loading matrices will be sampled from the spike or slab depending on these indicators. Accordingly, it is reasonable to enforce that the h^{th} factor $\eta_{\cdot h}$ is included in the shared variation part of equation (3) if and only if the corresponding loadings are active in at least two components of the model, either 2+ views or 1+ view and the response. To maintain increasing shrinkage across the columns of the loadings matrices to adaptively select the correct number of shared factors, we set

$$\begin{aligned} \psi_{mh} &= \mathbb{P}\left[\{\delta_{mh} > h\} \cap \left\{\{\delta_h = 1\} \cup \left\{\bigcup_{m' \neq m} \{\delta_{m'h} > h\}\right\}\right\}\right] \\ &= \mathbb{P}[\delta_{mh} > h] \mathbb{P}\left[\{\delta_h = 1\} \cup \left\{\bigcup_{m' \neq m} \{\delta_{m'h} > h\}\right\}\right] \\ &= \mathbb{P}[\delta_{mh} > h] \left(1 - \mathbb{P}\left[\{\delta_h = 0\} \cap \left\{\bigcap_{m' \neq m} \{\delta_{m'h} \leq h\}\right\}\right]\right) \\ &= \mathbb{P}[\delta_{mh} > h] \left(1 - \mathbb{P}[\delta_h = 0] \prod_{m' \neq m} \mathbb{P}[\delta_{m'h} \leq h]\right) \end{aligned}$$

and

$$\psi_h = \mathbb{P}\left[\{\delta_h = 1\} \cap \left\{\bigcup_{m'} \{\delta_{m'h} > h\}\right\}\right] = \mathbb{P}[\delta_h = 1] \left(1 - \prod_{m'} \mathbb{P}[\delta_{m'h} \leq h]\right),$$

while, analogously to the original CUSP construction, a priori we set

$$\begin{aligned} \mathbb{P}[\delta_{mh} = l] &= \xi_{ml} & \xi_{mh} &= \rho_{mh} \prod_{l=1}^{h-1} (1 - \rho_{ml}) & \rho_{mh} &\sim \mathcal{B}e(1, \alpha_m^{(\Lambda)}) \\ \mathbb{P}[\delta_h = 0] &= \xi & \xi &\sim \mathcal{B}e(a^{(\xi)}, b^{(\xi)}). \end{aligned}$$

We refer to the resulting prior as the dependent CUSPs (D-CUSP) prior. Coherently with the rationale above, the probability of any shared factor $\eta_{\cdot h}$ being inactive can be expressed as

$$\begin{aligned} \mathbb{P}[\eta_{\cdot h} \text{ inactive}] &= \mathbb{P}[\mathbb{1}_{(\delta_h=1)} + \sum_m \mathbb{1}_{(\delta_{mh} > h)} \leq 1] \\ &= \mathbb{P}[\mathbb{1}_{(\delta_h=1)} + \sum_m \mathbb{1}_{(\delta_{mh} > h)} = 0] + \mathbb{P}[\mathbb{1}_{(\delta_h=1)} + \sum_m \mathbb{1}_{(\delta_{mh} > h)} = 1] \\ &= \mathbb{P}[\delta_h = 0] \prod_m \mathbb{P}[\delta_{mh} \leq h] + \mathbb{P}[\delta_h = 1] \prod_m \mathbb{P}[\delta_{mh} \leq h] + \mathbb{P}[\delta_h = 0] \mathbb{P}[\sum_m \mathbb{1}_{(\delta_{mh} > h)} = 1] \\ &= \prod_m \mathbb{P}[\delta_{mh} \leq h] + \mathbb{P}[\delta_h = 0] \sum_m \mathbb{P}[\delta_{mh} > h] \prod_{m' \neq m} \mathbb{P}[\delta_{m'h} \leq h]. \end{aligned}$$

The above quantity can be used to compute the prior expectation for the number of shared factors K_o , which is helpful in eliciting hyperparameters α_m of the stick-breaking process:

$$\begin{aligned} \mathbb{E}[K_o] &= \mathbb{E}\left[\sum_{h=1}^{\infty} (1 - \mathbb{P}[\boldsymbol{\eta}_{\bullet,h} \text{ inactive}])\right] \\ &= \sum_{h=1}^{\infty} \left(1 - \prod_{m=1}^M \left(1 - \left(\frac{\alpha_m}{1 + \alpha_m}\right)^h\right) - \frac{a^{(\xi)}}{a^{(\xi)} + b^{(\xi)}} \sum_{m=1}^M \left(\frac{\alpha_m}{1 + \alpha_m}\right)^h \prod_{m' \neq m} \left(1 - \left(\frac{\alpha_{m'}}{1 + \alpha_{m'}}\right)^h\right)\right). \end{aligned}$$

Contrarily to the original CUSP construction, $\mathbb{E}[K_o]$ does not admit a closed-form expression, although it can be trivially computed for any values of the hyperparameters. As before, we consider a truncated version of the D-CUSP construction for practical reasons, by setting a suitable finite upper bound K on the number of shared factors. The hyperparameter K can still be tuned adaptively in the Gibbs sampler, where now we drop the columns of $\boldsymbol{\theta}$ and of all $\{\boldsymbol{\Lambda}_m\}_m$ that are either active for only one component of the model or inactive in all of them.

2.2.2 Identifiability of effectively shared factors under D-CUSP

The proposed D-CUSP construction induces the identification of shared and view-specific latent factors in additive factor models for multiview data. The D-CUSP prior puts zero mass on any configuration in which any h^{th} column of the loadings has signals in only one view, while that of all other views and the response are inactive. Such a property is particularly desirable in healthcare applications, such as in Section 4, given the interest in reliable identification of clinically actionable biomarkers. Unstructured priors for the loadings matrix of the shared component, such as BFSP or JAFAR under independent CUSP priors on each view, face practical problems due to their lack of identification restriction. For example, our empirical analyses show that, under independent CUSP priors on the loadings $\boldsymbol{\Lambda}_m$, the posterior distribution tends to always saturate at the maximum number of allowed shared factors, even for large upper bounds. This is intuitive given that nominally shared factors have more descriptive power than view-specific ones. Interestingly, our results suggest that the negative consequences of such an issue are not only limited to the mixing of the MCMC chain. Indeed, improper factor allocation is empirically associated with a worse fit to the multiview data, compared to that for the proposed D-CUSP prior.

2.3 Posterior inference via partially collapsed Gibbs sampler

Under the proposed extension of the CUSP construction to the multiview case, the linear-response version of JAFAR still allows for straightforward Gibbs sampling via conjugate full conditionals. Most of the associated full conditionals take the same forms as those of a regular factor regression model under the CUSP prior. The main difference concerns sampling the latent indicators for the loadings matrix in the shared component of the model. The latter can potentially be sampled jointly from $\mathbb{P}[\delta_h = s_h, \{\delta_{mh} = s_{mh}\}_{m=1}^M \mid -]$ for each $h = 1, \dots, K$, where the hyphen “ $-$ ” is a shorthand to specify the conditioning on all other variables, while $s_h \in \{0, 1\}$ and $s_{mh} \in \{1, \dots, K\}$. This would entail the evaluation of $K \cdot (2 \cdot K^M)$ probabilities for each Gibbs sampler iteration. We instead suggest targeting sequentially $\mathbb{P}[\delta_h = s_h \mid \{\delta_{mh} = s_{mh}\}_{m=1}^M, -]$ and $\mathbb{P}[\delta_{mh} = s_{mh} \mid \{\delta_h = s_h, \{\delta_{m'h} = s_{m'h}\}_{m' \neq m}, -]$, cutting down the number of required probabilities to $K \cdot (2 + K \cdot M)$. We found the associated efficiency gain and mixing loss trade-off to be greatly beneficial in practical applications.

Although Gibbs sampling is simple to implement, simple one-at-a-time updates can face slow mixing in factor models. We propose two modifications to head off such problems, leading to a partially collapsed Gibbs sampler (Park & van Dyk 2009).

Joint sampling of shared and view-specific loadings

First, for each $m = 1, \dots, M$ and $j = 1, \dots, p_{m,j}$ $[\boldsymbol{\Lambda}_{mj\bullet}, \boldsymbol{\Gamma}_{mj\bullet}]$ are sampled jointly from a $(K + K_m)$ -dimensional normal distribution. Conducting similar joint updates under the BSFP model for coefficients $[\boldsymbol{\theta}_0^\top, \boldsymbol{\theta}_1^\top, \dots, \boldsymbol{\theta}_M^\top]^\top$ has the $(K + \sum_{m=1}^M K_m)^3$ cost of sampling from a $(K + \sum_{m=1}^M K_m)$ -dimensional normal. The JAFAR structure naturally overcomes this issue, since sampling the coefficients $\boldsymbol{\theta}$ requires only dealing with a K -dimensional normal at K^3 cost.

Marginalization of view-specific factors

Secondly, the partially collapsed nature of the proposed Gibbs sampler arises from the update of the latent factors. In fact, for each $i = 1, \dots, n$, a standard Gibbs sampler would sample them sequentially from $\mathbb{P}[\boldsymbol{\eta}_i | \{\phi_{mi}\}_{m=1}^M, -]$ and $\mathbb{P}[\phi_{mi} | \boldsymbol{\eta}_i, \{\phi_{m'i}\}_{m' \neq m}, -]$, for each $m = 1, \dots, M$. We instead sample jointly via blocking and marginalization, exploiting the factorization

$$\mathbb{P}[\boldsymbol{\eta}_i, \{\phi_{mi}\}_{m=1}^M | -] = \mathbb{P}[\{\phi_{mi}\}_{m=1}^M | \boldsymbol{\eta}_i, -] \mathbb{P}[\boldsymbol{\eta}_i | -] = \left(\prod_{m=1}^M \mathbb{P}[\phi_{mi} | \boldsymbol{\eta}_i, -] \right) \mathbb{P}[\boldsymbol{\eta}_i | -].$$

Here $\mathbb{P}[\boldsymbol{\eta}_i | -]$ denotes the full conditional of the shared factors in a collapsed version of the model, where all view-specific factors have been marginalized out. The structure of JAFAR facilitates the marginalization of the ϕ_{mi} 's. In contrast, the interdependence created by the response component in BSFP leads to a $\mathcal{O}((\sum_{m=1}^M K_m)^3)$ cost for the update of $\mathbb{P}[\boldsymbol{\eta}_i | -]$, as opposed to the $\mathcal{O}(\sum_{m=1}^M K_m^3)$ for JAFAR. Furthermore, the term $\mathbb{P}[\{\phi_{mi}\}_{m=1}^M | \boldsymbol{\eta}_i, -]$ does not factorize over m in BSFP, still due to the response part, leading to a second $\mathcal{O}((\sum_{m=1}^M K_m)^3)$ -cost update.

The same rationale applies to the extensions of JAFAR presented in Appendix C, addressing flexible response modeling via interaction terms and splines. In such cases, the conditional conjugacy of the specific factors is preserved, while the shared factors can be sampled via a Metropolis-within-Gibbs step targeting the associated full conditional in the collapsed model.

2.4 Postprocessing and Multiview MatchAlign

Despite having addressed the identifiability of shared versus view-specific factors, the loading matrices still suffer from rotational ambiguity, label switching and sign switching. These are notorious issues of latent factor models, particularly within the Bayesian paradigm (Poworoznek et al. 2021). Indeed, it is easy to verify that the induced joint covariance decomposition is not unique. Consider semi-orthogonal matrices \mathbf{R} and $\{\mathbf{P}_m\}_m$, respectively of dimensions $K \times K$ and $\{K_m \times K_m\}_m$. Then, the transformed set of loadings $\ddot{\mathbf{\Lambda}}_m = \mathbf{\Lambda}_m \mathbf{R}$ and $\ddot{\mathbf{\Gamma}}_m = \mathbf{\Gamma}_m \mathbf{P}_m$ clearly satisfy $\ddot{\mathbf{\Lambda}}_m \ddot{\mathbf{\Lambda}}_{m'}^\top = \mathbf{\Lambda}_m \mathbf{\Lambda}_{m'}^\top$, and $\ddot{\mathbf{\Gamma}}_m \ddot{\mathbf{\Gamma}}_{m'}^\top = \mathbf{\Gamma}_m \mathbf{\Gamma}_{m'}^\top$, for every $m, m' = 1, \dots, M$, which leaves $\text{cov}(\mathbf{x}_m)$ and $\text{cov}(\mathbf{x}_m, \mathbf{x}_{m'})$ unaffected. Concurrently, adequately transforming $\boldsymbol{\theta}$ and $\boldsymbol{\eta}_i$ to $\tilde{\boldsymbol{\theta}} = \boldsymbol{\theta} \mathbf{R}$ and $\tilde{\boldsymbol{\eta}}_i = \mathbf{R}^\top \boldsymbol{\eta}_i$ preserves predictions of the response y_i . Such non-identifiability is particularly problematic when there is interest in inferring the latent variables and corresponding factor loadings. Several contributions in the literature have addressed this problem. MatchAlign (Poworoznek et al. 2021) provides an efficient post-processing algorithm, which first applies Varimax (Kaiser 1958) to every loadings sample to orthogonalize, fixing optimal rotations according to a suitable objective function. While this solves rotational ambiguity, the loadings samples still suffer from non-identifiability with respect to column labels and sign switching. Accordingly, the authors propose to address both issues in a second step, by matching and aligning each posterior sample to a reference via a greedy maximization procedure.

Multiview Varimax

To address rotational ambiguity, label switching and sign switching, MatchAlign could be applied to MCMC samples of the stacked loadings matrices $\mathbf{\Lambda} = [\mathbf{\Lambda}_1^\top, \dots, \mathbf{\Lambda}_M^\top, \boldsymbol{\theta}_0^\top]^\top$ and view-specific $\mathbf{\Gamma}_m = [\mathbf{\Gamma}_m, \boldsymbol{\theta}_m^\top]^\top$, for each $m = 1, \dots, M$. However, a more elaborate approach can be beneficial in multiview scenarios. A side-benefit of Varimax is inducing row-wise sparsity in the loadings matrices, which in turn allows for clearer interpretability of the role of different latent sources of variability. This is because, given any $p \times K$ loading matrix $\mathbf{\Lambda}$, the Varimax procedure solves the optimization problem $\mathbf{R}_o = \underset{\mathbf{R} \in \mathbb{R}^{K \times K}: \mathbf{R} \mathbf{R}^\top = \mathbf{I}_K}{\text{argmax}} V(\mathbf{\Lambda}, \mathbf{R})$, where

$$V(\mathbf{\Lambda}, \mathbf{R}) = \frac{1}{p} \sum_{h=1}^K \sum_{j=1}^p (\mathbf{\Lambda} \mathbf{R})_{jh}^4 - \sum_{h=1}^K \left(\frac{1}{p} \sum_{j=1}^p (\mathbf{\Lambda} \mathbf{R})_{jh}^2 \right)^2.$$

Accordingly, \mathbf{R}_o is the optimal rotation matrix maximizing the sum of the variances of the squared loadings. Intuitively, this is achieved under two conditions. First, any given \mathbf{x}_j has large loading $\mathbf{\Lambda}_{jh^*}$ on a single factor h^* , but near-zero loadings $\mathbf{\Lambda}_{j-h^*}$ on the remaining $K - 1$ factors. Secondly, any h^{th} factor is loaded on by only a small subset $\mathcal{J}_h \subset \{1, \dots, p\}$ of variables, having high loadings $\mathbf{\Lambda}_{\mathcal{J}_h h}$ on such a factor, while the loadings $\mathbf{\Lambda}_{-\mathcal{J}_h h}$ associated with the remaining $\{1, \dots, p\} \setminus \mathcal{J}_h$ variables are close to zero. However, when

applied to the stacked shared loadings of JAFAR or BSFP, such a sparsity-inducing mechanism can disrupt the very structure for which the models were designed. This is because a naive application of `Varimax` to the stacked loadings is likely to favor representations in which each factor is effectively loaded only by a subset of variables \mathbf{x}_m from a single view, in an effort to minimize the cardinality of $|\mathcal{J}_h|$ for every $h = 1, \dots, K$. This destroys the interpretation of shared factors as latent sources of variations affecting multiple components of the data.

Hence, we suggest instead solving $\mathbf{R}_* = \operatorname{argmax}_{\mathbf{R} \in \mathbb{R}^{K \times K}: \mathbf{R}\mathbf{R}^\top = \mathbf{I}_K} \sum_{m=1}^M V(\mathbf{\Lambda}_m, \mathbf{R})$, with

$$\sum_{m=1}^M V(\mathbf{\Lambda}_m, \mathbf{R}) = \sum_{m=1}^M \left(\frac{1}{p_m} \sum_{h=1}^K \sum_{j=1}^{p_m} (\mathbf{\Lambda}_m \mathbf{R})_{jh}^4 - \sum_{h=1}^K \left(\frac{1}{p_m} \sum_{j=1}^{p_m} (\mathbf{\Lambda}_m \mathbf{R})_{jh}^2 \right)^2 \right) \quad (6)$$

representing the sum of the within-view squared loadings sum of variances, after applying any rotation \mathbf{R} . Accordingly, this is expected to enforce sparsity within each view, but not across views. Optimization of the modified target entails trivial modification of the original routine.

2.5 Modeling extensions: flexible data representations

Equation (3) can be viewed as the main building block of more complex modeling formulations, allowing greater flexibility in the descriptions of both the multiview data and the response component. Here we address deviations from normality in the multiview data, which is a fragile assumption in Gaussian factor models. In many applications, such as multi-omics data, the features are often non-normally distributed, right-skewed, and can have a significant percentage of measurements below the limit of detection (LOD) or of missing data. The latter might also come in blocks, with certain modalities only measured for subgroups of the subjects. All factor model formulations allow trivially dealing with missing data and LOD, adding an imputation step to the MCMC algorithm or marginalizing them out. Nonetheless, Gaussian formulations as in equations (3) and (2) demand that the latent factor decomposition simultaneously describe the dependence structure and the marginal distributions of the features. This can negatively affect the performance of the methodology, while having a confounding effect on the identification of latent sources of variation. To address this issue, we develop a copula factor model extension of JAFAR (Hoff 2007, Murray et al. 2013, Feldman & Kowal 2023), which allows us to disentangle learning of the dependence structure from that of margins. Notably, the D-CUSP prior structure described above readily applies to such extensions as well.

Non-Gaussian data: single-view case & copula factor regression

For ease of exposition, we first introduce Copula Factor Models in the simplified case of a single set of features $\mathbf{x}_i \in \mathbb{R}^p$, before extending to the multiview case. Adhering to the formulation in (Hoff 2007), we model the joint distribution of \mathbf{x}_i as $F(\mathbf{x}_{i1}, \dots, \mathbf{x}_{ip}) = \mathcal{C}(F_1(\mathbf{x}_{i1}), \dots, F_p(\mathbf{x}_{ip}))$, where F_j is the univariate marginal distribution of the j^{th} entry, and $\mathcal{C}(\cdot)$ is a distribution function on $[0, 1]^p$ that describes the dependence between the variables. Any joint distribution F can be completely specified by its marginal distributions and a copula \mathcal{C} (Sklar 1959), with the copula being uniquely determined when the variables are continuous. Here we employ the Gaussian Copula $\mathcal{C}(u_1, \dots, u_p) = \Phi_p(\Phi^{-1}(u_1), \dots, \Phi^{-1}(u_p) | \mathbf{\Sigma})$, where $\Phi_p(\cdot | \mathbf{\Sigma})$ is the p -dimensional Gaussian cdf with correlation matrix $\mathbf{\Sigma}$, $\Phi(\cdot)$ is the univariate standard Gaussian cdf and $[u_1, \dots, u_p] \in [0, 1]^p$. Plugging in the Gaussian copula in the general formulation, the implied joint distribution of \mathbf{x}_i is

$$F(\mathbf{x}_{i1}, \dots, \mathbf{x}_{ip}) = \Phi_p\left(\Phi^{-1}(F_1(\mathbf{x}_{i1})), \dots, \Phi^{-1}(F_p(\mathbf{x}_{ip})) \mid \mathbf{\Sigma}\right).$$

Hence, the Gaussian distribution is used to model the dependence structure, whereas the data have univariate marginal distributions $F_j(\cdot)$. The Gaussian copula model is conveniently rewritten via a latent variable representation, such that $\mathbf{x}_{ij} = F_j^{-1}(\Phi(\mathbf{z}_{ij}/c_j))$, with $\mathbf{z}_i \sim N_p(\mathbf{0}_p, \mathbf{\Sigma})$. Here $F_j^{-1}(\cdot)$ is the pseudo-inverse of the univariate marginal of the j^{th} entry, \mathbf{z}_{ij} is the latent variable related to predictor j and observation i , and c_j is a positive normalizing constant. Following (Murray et al. 2013), the learning of the potentially large correlation structure $\mathbf{\Sigma}$ can proceed by endowing \mathbf{z}_i with a latent factor model $\mathbf{z}_i \sim N_p(\mathbf{\Lambda}\boldsymbol{\eta}_i, \mathbf{D})$, with $\mathbf{D} = \operatorname{diag}(\{\sigma_j^2\}_{j=1}^p)$, $p \times k$ factor loadings matrix $\mathbf{\Lambda}$ and latent factors $\boldsymbol{\eta}_i \sim N_K(\mathbf{0}_K, \mathbf{I}_K)$. Likewise, predictions of a continuous health outcome y_i can be accounted for via a regression on the latent factors

$y_i \sim N(f(\boldsymbol{\eta}_i), \sigma_y^2)$, where in JAFAR we consider a simple linear mapping $f(\boldsymbol{\eta}_i) = \boldsymbol{\theta}^\top \boldsymbol{\eta}_i$. In the latter case, the induced regression is linear also in \mathbf{z}_i :

$$\begin{aligned} \mathbb{E}[y_i | \mathbf{x}_i] &= \mathbb{E}[\boldsymbol{\theta}^\top \boldsymbol{\eta}_i | \mathbf{x}_i] = \boldsymbol{\theta}^\top \mathbb{E}[\boldsymbol{\eta}_i | \mathbf{x}_i] = \boldsymbol{\theta}^\top \mathbb{E}[\mathbb{E}[\boldsymbol{\eta}_i | \mathbf{z}_i] | \mathbf{x}_i] \\ &= \boldsymbol{\theta}^\top \mathbb{E}[(\boldsymbol{\Lambda}^\top \mathbf{D}^{-1} \boldsymbol{\Lambda} + \mathbf{I}_K)^{-1} \boldsymbol{\Lambda}^\top \mathbf{D}^{-1} \mathbf{z}_i | \mathbf{x}_i] = \boldsymbol{\theta}^\top \mathbf{A} \mathbb{E}[\mathbf{z}_i | \mathbf{x}_i], \end{aligned}$$

where $\mathbb{E}[\mathbf{z}_i | \mathbf{x}_i]$ is a vector such that the j^{th} element is equal to $c_j \Phi^{-1}(F_j(\mathbf{x}_{ij}))$. This follows from the fact that the distribution of $\boldsymbol{\eta}_i | \mathbf{z}_i$ is normal with covariance $\mathbf{V} = (\boldsymbol{\Lambda}^\top \mathbf{D}^{-1} \boldsymbol{\Lambda} + \mathbf{I}_K)^{-1}$ and mean $\mathbf{A} \mathbf{z}_i$ where $\mathbf{A} = \mathbf{V} \boldsymbol{\Lambda}^\top \mathbf{D}^{-1}$. To enforce standardization of the latent variables, $c_j = \sqrt{\sigma_j^2 + \sum_{h=1}^k \boldsymbol{\Lambda}_{jh}^2}$, which would non-trivially complicate the sampling process. However, since the model is invariant to monotone transformations (Murray et al. 2013), we can use instead

$$\mathbf{x}_{ij} = F_j^{-1}(\Phi(\mathbf{z}_{ij})) \quad \mathbf{z}_i \sim N_p(\boldsymbol{\Lambda} \boldsymbol{\eta}_i, \mathbf{D}) \quad \eta_i \sim N(\mathbf{0}_K, \mathbf{I}_K).$$

The only element left to be addressed is the estimation of the marginal distributions F_j . In many practical scenarios, the features are continuous, or treated as such with negligible impact on the overall analysis. In such a setting, it is common to replace $F_j(\cdot)$ by the scaled empirical marginal cdf $\hat{F}_j(t) = \frac{n}{n+1} \sum_{i=1}^n \frac{1}{n} \mathbb{1}(\mathbf{x}_{ij} \leq t)$, benefiting from the associated theoretical properties (Klaassen et al. 1997). Alternatively, Hoff (2007) and Murray et al. (2013) viewed the marginals as nuisance parameters and targeted learning of the copula correlation for mixed data types via extended rank likelihood. Recently, Feldman & Kowal (2023) proposed an extension for fully Bayesian marginal distribution estimation, with remarkable computational efficiency for discrete data.

Non-Gaussian data: multiview case

Extending the same rationale to the multiview case, the copula factor model now targets the joint distribution of $\mathbf{x} = [\mathbf{x}_{1i}^\top, \dots, \mathbf{x}_{Mi}^\top]^\top$ as

$$F(\mathbf{x}_{1i}, \dots, \mathbf{x}_{Mi}) = \mathcal{C}(F_{11}(x_{1i1}), \dots, F_{1p_1}(x_{1ip_1}), \dots, F_{M1}(x_{Mi1}), \dots, F_{Mp_M}(x_{Mip_M})).$$

Here $p = \sum_{m=1}^M p_m$, while F_{mj} is the univariate marginal cdf of the j^{th} variable in the m^{th} view. The additive latent factor structure from equation (3) can be directly imposed on the transformed variables $\mathbf{z}_i = [\mathbf{z}_{1i}^\top, \dots, \mathbf{z}_{Mi}^\top]^\top$, introducing again the distinction between shared and view-specific factors. The overall model formulation becomes

$$\begin{aligned} \mathbf{x}_{mij} &= F_{mj}^{-1}(\Phi(\mathbf{z}_{mij})) \\ \mathbf{z}_{mi} &= \boldsymbol{\mu}_m + \boldsymbol{\Lambda}_m \boldsymbol{\eta}_i + \boldsymbol{\Gamma}_m \boldsymbol{\phi}_{mi} + \boldsymbol{\epsilon}_{mi} \\ y_i &= \mu_y + \boldsymbol{\beta}^\top \mathbf{r}_i + \boldsymbol{\theta}^\top \boldsymbol{\eta}_i + e_i. \end{aligned} \tag{7}$$

As before, F_{mj}^{-1} is the pseudo-inverse of F_{mj} . Missing data can be imputed by sampling the corresponding entries $\tilde{\mathbf{z}}_{mij} \sim \mathcal{N}(\boldsymbol{\mu}_m + \boldsymbol{\Lambda}_{mj}^\top \boldsymbol{\eta}_i + \boldsymbol{\Gamma}_{mj}^\top \boldsymbol{\phi}_{mi}, \boldsymbol{\sigma}_{mj}^2)$ at each iteration of the sampler. When there is no direct interest in reconstructing the missing data, subject-wise marginalization of the missing entries can improve mixing compared to their imputation.

3 Simulation Studies

To assess the performance of JAFAR under the D-CUSP prior, we first conducted simulation experiments. These experiments involved generating data from a factor model with the additive structure outlined in equation (3). We considered 10 independent replicated datasets, each with $M = 3$ views of dimensions $p_m = \{100, 200, 300\}$, for increasing sample sizes $n \in \{50, 100, 200, 500\}$ and fixed test set size $n_{\text{test}} = 100$. Such values were chosen to preserve a $p \gtrsim n$ setup and to create challenging test cases. The assumed number of shared factors was set to $K^{(\text{true})} = 15$, with the responses loading on 9 of them, while the view-specific ones were $\{K_m^{(\text{true})}\}_{m=1}^M = \{8, 9, 10\}$. To create realistic simulations that mimic real-world multiview data, we propose a novel scheme for generating loading matrices. These matrices induce sensible block-structured correlations, as described in Appendix D. To test the identification of prediction-relevant features, only half of the features from each view were allowed to have non-zero loadings on response-related factors.

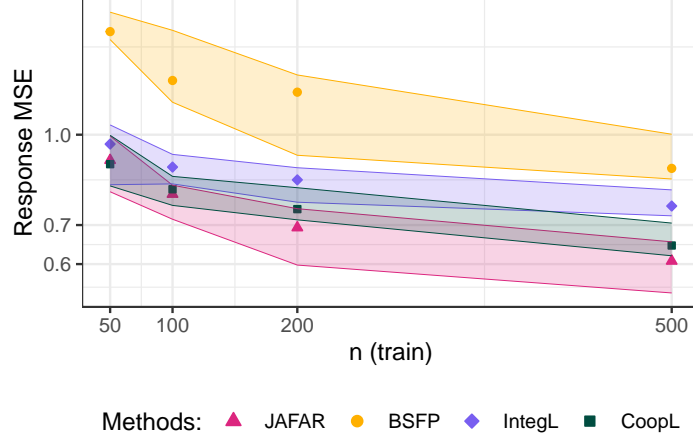


Figure 1: Mean squared error (in logarithmic scale) of the predicted responses in the test sets of simulated data. The x-axis reports increasing size of the train set. The interior points and band edges correspond to the quartiles over 10 independent replicates for fixed dimensions.

Given the generated the loading matrices $\mathbf{\Lambda}_m$ and $\mathbf{\Gamma}_m$, we sample the target signal-to-noise ratios $\{\text{snr}_{mj}\}_{j=1}^{p_m}$ from an inverse gamma distribution $\text{Inv}\mathcal{G}a(10, 30)$, and set accordingly each idiosyncratic variances to $\sigma_{mj}^2(\mathbf{\Lambda}_m\mathbf{\Lambda}_m^\top + \mathbf{\Gamma}_m\mathbf{\Gamma}_m^\top)_{jj}/\text{snr}_{mj}$, $\forall j = 1, \dots, p_m$. Analogous to the loading matrices generation from Appendix D, the absolute value of the active response coefficients θ_h was sampled from a beta distribution $\mathcal{B}e(5, 3)$, and their signs were randomly assigned with equal probability. The response variance σ_y^2 was adjusted such that the signal-to-noise ratio $\boldsymbol{\theta}^\top \boldsymbol{\theta} / \sigma_y^2$ equals 1. Both the multiview features and the response were standardized before the analysis to have mean zero and unit variance.

We compare JAFAR to BSFP; their paper provided a recent comparison to alternative latent factorization approaches showing state-of-the-art performance (Samorodnitsky et al. 2024). We also consider two other non-factor alternatives: Cooperative Learning (CoopLearn) and IntegratedLearner (IntegLearn). CoopLearn complements usual squared-error loss-based predictions with an agreement penalty, which encourages predictions coming from separate data views to match with one another. We set the associated agreement parameter to $\rho_{\text{CL}} = 0.5$. IntegLearn combines the predictions of Bayesian additive regression trees (BART) fit separately to each view, where we use the default late fusion scheme to integrate the individual models. The Gibbs samplers of JAFAR and BSFP were run for a total of $T_{\text{MCMC}} = 4000$ iterations, with a burn-in of $T_{\text{BURN-IN}} = 2000$ steps and thinning every $T_{\text{thin}} = 10$ samples for memory efficiency. We initialized the number of factors in JAFAR to $K^{(0)} = K^{\text{MAX}} = 40$ and $\{K_m^{(0)}\}_{m=1}^M = \{K_m^{\text{MAX}}\}_{m=1}^M = \{30, 30, 30\}$.

The hyperparameters of the D-CUSP prior were set to the values in Table 1. The prior parameters for σ_y^2 and σ_m^2 are meant to favor small values for σ_y^2 , inducing the model to explain a substantial part of the variability through the signal components rather than via noise. The hyperparameters of the spike-and-slab on the loadings are essentially a shrunk version of the ones suggested by Legramanti et al. (2020). In

Data distributions:

$$v_y^2 = v_m^2 = 4 \quad a^{(y)} = a^{(m)} = 3 \quad b^{(y)} = b^{(m)} = 1$$

Spike & slab variances:

$$\alpha_m^{(\Gamma)} = \alpha_m^{(\Lambda)} = a^{(\theta)} = 0.5 \quad b_m^{(\Gamma)} = b_m^{(\Lambda)} = b^{(\theta)} = 0.1 \quad \tau_{m\infty}^2 = \chi_{m\infty}^2 = \chi_\infty^2 = 0.005$$

Spike & slab weights:

$$\alpha_m^{(\Gamma)} = \alpha_m^{(\Lambda)} = 5 \quad a^\xi = 3 \quad b^\xi = 2$$

Table 1: D-CUSP hyperparameters values used in the empirical study from Section 4.

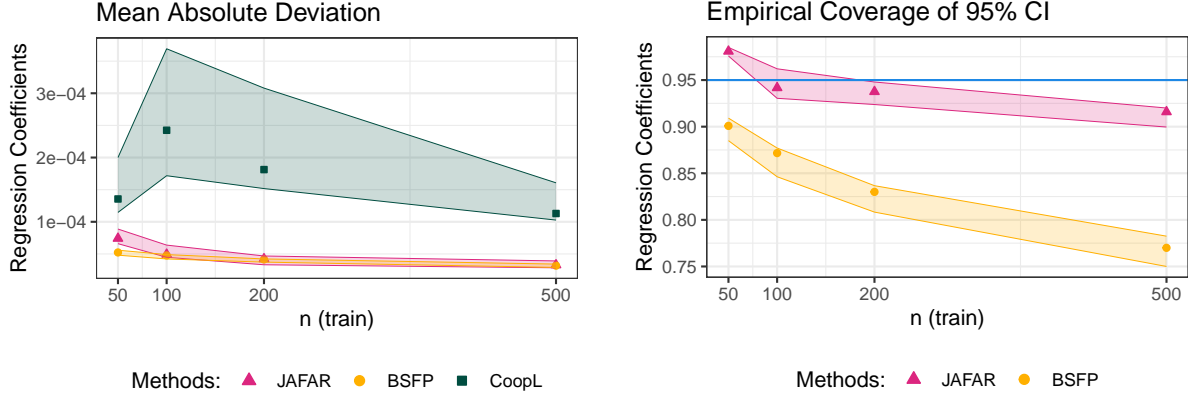


Figure 2: Inferred coefficients in the simulated data. The two columns report the mean absolute deviations and the empirical coverage of the 95% confidence intervals. The interior points and band edges correspond to the quartiles over 10 independent replicates for fixed dimensions. On the right, the horizontal blue corresponds to the correct coverage.

high-dimensional scenarios, our empirical results suggest that better performances are achieved by inducing smaller values of the loadings both for active and inactive columns, while still allowing for a clear separation of the two components. Notably, the proposed set of parameters leads to superior feature reconstructions for CUSP itself when applied to each separate view in the absence of the response. The choice of a^ξ and b^ξ reflects a slight prior preference for the active entries θ_h in the response loadings, rather than inactive, without increasing shrinkage on h .

In this setting, JAFAR achieves better prediction than all other methods, as shown in Figure 1. This stems from the more reliable reconstruction of the dependence structure underlying the data, both in terms of induced regression coefficients for $p(y_i | \mathbf{X}_{mi}^M_{m=1})$ and correlations in the multiview predictors. BSFP achieves competitive mean absolute deviations from the true regression coefficients. However, this appears to be due to the BSFP model overshrinking the coefficient estimates, as suggested by Figure A2 and the other results presented in Appendix A.

In Figure 3, we analyzed accuracy in capturing the dependence structure in the multiview features. We focus on the Frobenius norm of the difference between the true and inferred correlation matrices across and within views, associated with equation (5). JAFAR provides a more reliable disentanglement of latent axes of variation, while BSFP suffers from overshrinking induced by the factors' prior variances r_o and r_m . This issue is only partly mitigated when considering the in-sample empirical correlations of draws from $p(\mathbf{X}_m | \mathbf{X}_{m' m' \neq m})$. The additional results from Appendix A show that the superior performance of JAFAR holds under the corresponding Frobenius norm as well.

Notice that out-of-sample predictions of $\mathbb{E}[y_i | \{\mathbf{X}_{mi}\}_{m=1}^M, -]$ can be easily constructed via Monte Carlo averages $\frac{1}{T_{\text{EFF}}} \sum_{t=1}^{T_{\text{EFF}}} \mathbb{E}[y_i | \boldsymbol{\eta}_i^{(t)} -]$ exploiting samples from $\boldsymbol{\eta}_i^{(t)} \sim p(\boldsymbol{\eta}_i | \{\mathbf{X}_{mi}\}_{m=1}^M, -)$, where T_{EFF} is the number of MCMC samples after burn-in and thinning. To ensure coherence in this analysis, we modified the function `bsfp.predict` from the main BSFP GitHub repository. Indeed, the default implementation considers only samples from $p(\boldsymbol{\eta}_i | y_i, \{\mathbf{X}_{mi}\}_{m=1}^M, -)$ and $p(\boldsymbol{\phi}_{mi} | y_i, \mathbf{X}_{mi}, -)$, i.e. conditioning on the response as well. The updated code is available in the JAFAR GitHub repository.

4 Labor onset prediction from immunome, metabolome & proteome

To further showcase the performance of the proposed methodology on real data, we focus on predicting time-to-labor onset from immunome, metabolome, and proteome data for a cohort of women who went into labor spontaneously. The dataset, available in the GitHub repository associated with Mallick et al. (2024), considers repeated measurements during the last 100 days of pregnancy for 63 women. Similar to Ding

et al. (2022), we obtained a cross-sectional sub-dataset by considering only the first measurement for each woman. We dropped 10 subjects for which only immunome data were available and split the remaining 53 observations into training and test sets of $n_{train} = 40$ and $n_{test} = 13$ subjects, respectively. The dataset falls into a large- p -small- n scenario, as the $M = 3$ layers of blood measurements provide information on $p_1 = 1141$ single-cell immune features, $p_2 = 3529$ metabolites, and $p_3 = 1317$ proteins.

As before, we compare JAFAR to BSFP, Cooperative Learning (CoopLearn) and the IntegratedLearner (IntegLearn), with the same hyperparameters from the previous section. The Gibbs samplers of JAFAR and BSFP were run for a total of $T_{MCMC} = 8000$ iterations, with a burn-in of $T_{BURN-IN} = 4000$ steps and thinning every $T_{thin} = 10$ samples for memory efficiency. We initialized the number of factors in JAFAR to $K^{(0)} = K^{MAX} = 60$ and $\{K_m^{(0)}\}_{m=1}^M = \{K_m^{MAX}\}_{m=1}^M = \{60, 60, 60\}$. Prior to analysis, we standardized the data and log-transformed the metabolomics and proteomics features. Despite these preprocessing steps, all omics layers exhibited considerable deviation from Gaussianity, with over 30% of features in each view yielding univariate Shapiro test statistics below 0.95. To address this challenge, we introduced copula factor model variants for both JAFAR and BSFP, as elaborated in Section 2.5. Given the continuous nature of the omics data without any missing entries, the incorporation of the copula layer can be construed as a deterministic preprocessing procedure, involving feature-wise transformations that leverage estimates of the associated empirical cumulative distribution functions.

The relative accuracy in predicting the response values is summarized in Figure 4. Compared to CoopLearn and IntegLearn, JAFAR achieves better predictive performance in both the training and test sets, while also demonstrating good coverage of the predictive intervals. As before, BSFP achieves substandard performance in capturing meaningful latent sources of variability associated with the response. This could partly be attributed to the limited number of factors inferred by the UNIFAC initialization, as depicted in Figure 5. JAFAR learns a substantially greater number of factors, particularly in the shared component of the model.

Most of the shared axes of variation learned by JAFAR are related to the variability in response, as demonstrated by the Venn diagram in Figure 5. The rightmost panel of Figure 6 further supports the intuition that such latent sources of variation capture underlying biological processes that affect the system as a whole. There, we summarize the squared error of JAFAR in predicting the response on the test set when holding out one entire omics layer at a time, indicating only a moderate effect on prediction accuracy. Figure 8 reports the posterior mean of the shared loading matrices after postprocessing using the extended version of

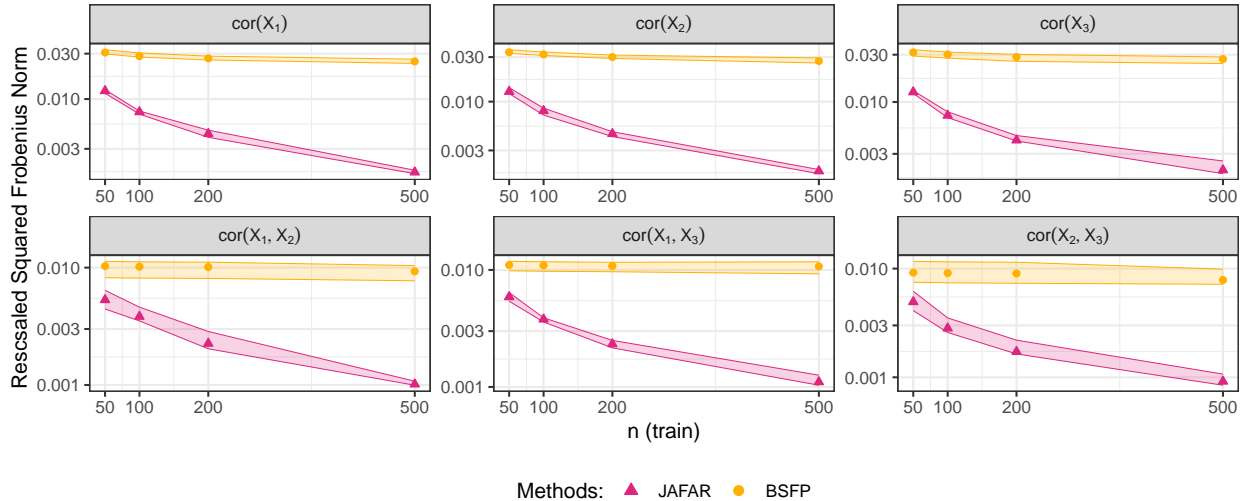


Figure 3: Frobenius norms of the differences between the true and inferred correlations for the simulated data. The two rows report the inter and intra-view correlations, respectively. All norms have been rescaled by the dimensions of the corresponding matrices. The interior points and band edges correspond to the quartiles over 10 independent replicates for fixed dimensions.

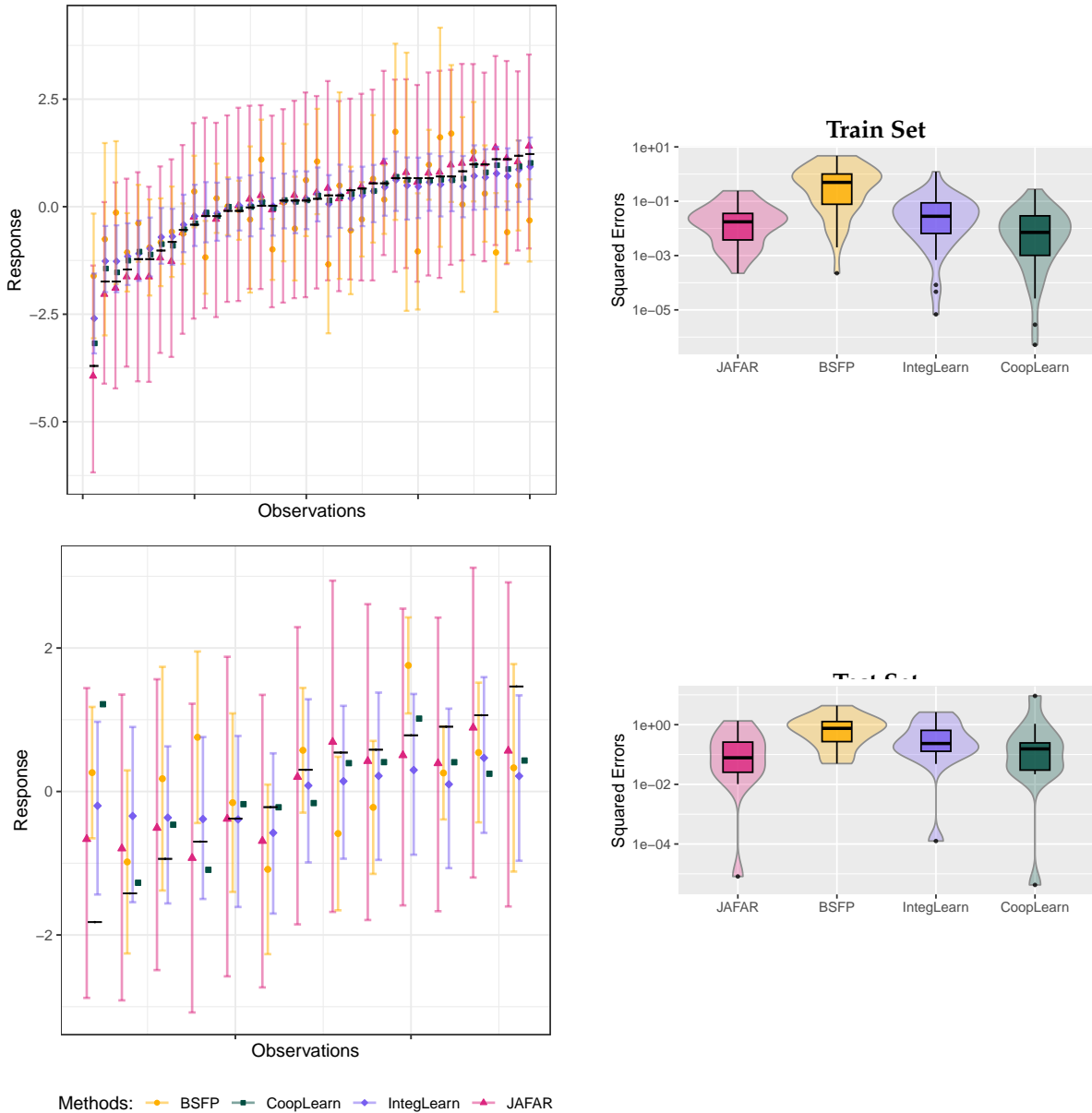


Figure 4: Response prediction accuracy for the different methods considered. In the plots to the left, the dots and the vertical bars represent the expected values and the 95% credible intervals for the predicted responses, respectively. The black horizontal ticks correspond to the true values of the response for each observation. Both *CoopLearn* and *IntegLearn* achieve good predictive performances in the train set, but do not perform as well on out-of-sample observations. *BSFP* performs worse both in terms of expected values and predictive intervals, which are almost as wide as the effective range of the response. *JAFAR* achieves remarkable generalization error on the test.

MatchAlign via Multiview Varimax. Similar to the simulation studies, *JAFAR*'s good performances carry over to the reconstructed dependence structures in the predictors. In Figure 7, we report the empirical and inferred within-view correlation matrices, crucial to ensure meaningful interpretability of the latent sources of variation. The observed slight overestimation of the correlation structure is not uncommon in extremely high-dimensional scenarios. We omit the *BSFP* results, as the associated inferred correlation matrices collapse to essentially diagonal structures.

	Γ_1	Γ_2	Γ_3	Λ	Θ	Λ_1	Λ_2	Λ_3
JAFAR	16.81	21.14	17.89	56.61	41.94	19.01	43.70	39.96
BSFP	13	14	10	9	9	9	9	9

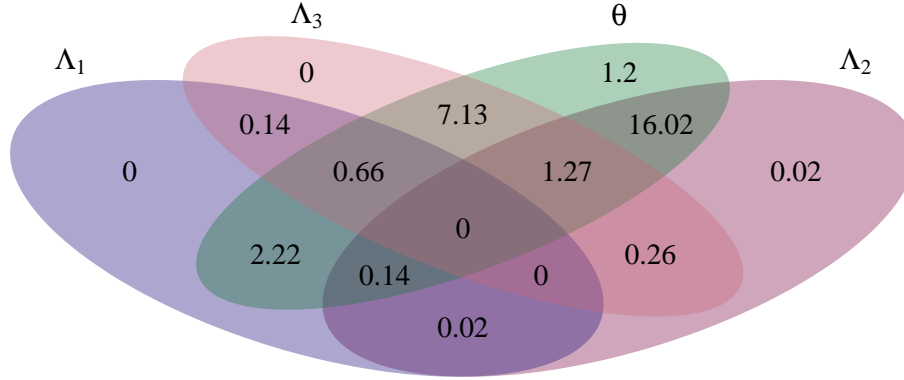


Figure 5: Inferred activity patterns in the specific and shared components loadings matrices $\{\Gamma_m\}_{m=1}^M$ and $\{\Lambda_m\}_{m=1}^M$ in the two additive factor models considered. Here the $M = 3$ omics layers correspond to immunome, metabolome and proteome data respectively. For BSFP, the reported values correspond to the fixed ranks inferred via the UNIFAC initialization. For JAFAR, they are posterior means of the number of active columns, according to the latent indicators in the D-CUSP construction. JAFAR further allows for composite activity patterns in the shared component of the model, as disentangled in the Venn diagram in the bottom part of the Figure.

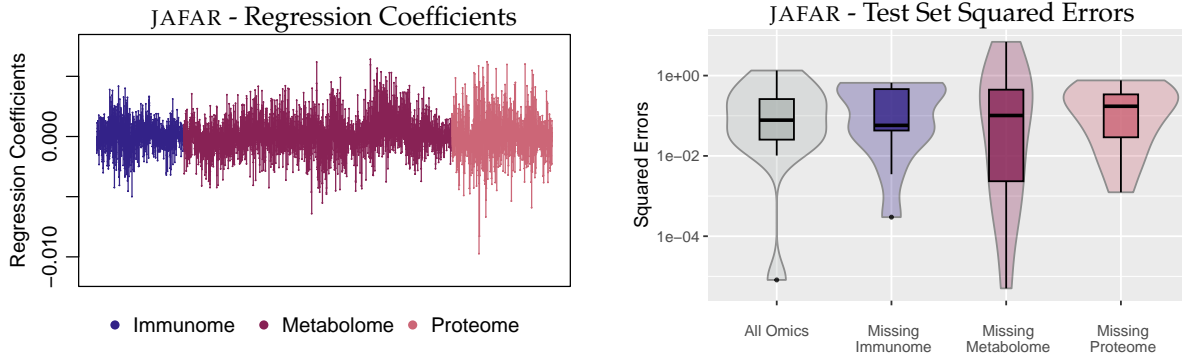


Figure 6: Induced linear regression coefficients for the response y_i on the omics data $\{\mathbf{x}_{mi}\}_m$ (left). The reported values correspond to the average over the MCMC chain. All three omics layers appear to be significant for prediction purposes, as confirmed by the leave-one-omics-out predictive squared errors (right). Prediction under an entirely missing omics layer is a straightforward task in factor models.

5 Discussion

We have developed a novel additive factor regression approach, termed JAFAR, for inferring latent sources of variability underlying dependence in multiview features. JAFAR isolates shared- and view-specific factors, thereby facilitating inference, prediction, and feature selection. To ensure the identifiability of shared sources of variation, we introduce a novel extension of the CUSP prior (Legramanti et al. 2020) and provide an enhanced partially collapsed Gibbs sampler for posterior inference. Additionally, we extend the Varimax procedure (Kaiser 1958) to multiview settings, preserving the composite structure of the model to resolve rotational ambiguity.

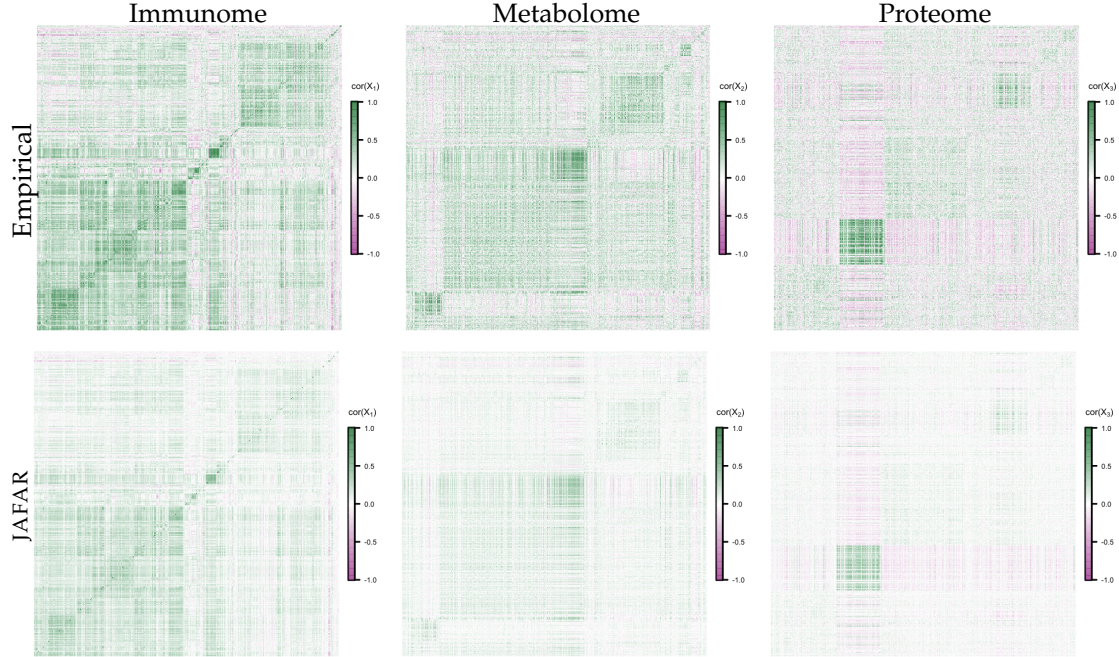


Figure 7: Empirical and inferred correlation structures for the three omics layers. The first row reports the empirical correlations on the train set. The second columns show the posterior mean of the correlation matrices associated with the induced covariances $\Lambda_m \Lambda_m^T + \Gamma_m \Gamma_m^T + \text{diag}(\sigma_m^2)$ inferred by JAFAR. JAFAR capture the main feature of the dependence structure, although suffering from a certain degree of underestimation. This issue is not uncommon in extremely high-dimensional scenarios, particularly with very few observations. Even run marginally on each omics from the dataset considered, the CUSP construction proved more effective in mitigating the severity of such an underestimation than other structured shrinkage priors for factor models, such as the Dirichlet-Laplace of the multiplicative gamma process.

JAFAR’s performance is compared to state-of-the-art competitors using multiview simulated data and in an application focusing on predicting time-to-labor onset from multiview features derived from immunomes, metabolomes, and proteomes. The carefully designed structure of JAFAR enables accurate learning and inference of response-related latent factors, as well as the inter- and intra-view correlation structures. In the appendix, we discuss more flexible response modeling through interactions among latent factors (Ferrari & Dunson 2021) and splines, while considering extensions akin to generalized linear models. The benefit of the proposed D-CUSP prior extends to unsupervised scenarios, particularly when the focus is solely on disentangling the sources of variability within integrated multimodal data. To the best of our knowledge, this results in the first fully Bayesian analog of JIVE (Lock et al. 2013). Lastly, analogous constructions can be readily developed using the structured increasing shrinkage prior proposed by Schiavon et al. (2022), allowing for the inclusion of prior annotation data on features.

Acknowledgements

This project has received funding from the European Research Council (ERC) under the European Union’s Horizon 2020 research and innovation program (grant agreement No 856506), and United States National Institutes of Health (R01ES035625, 5R01ES027498-05, 5R01AI167850-03), and was supported in part by Merck & Co., Inc., through its support for the Merck Biostatistics and Research Decision Sciences (BARDS) Academic Collaboration.

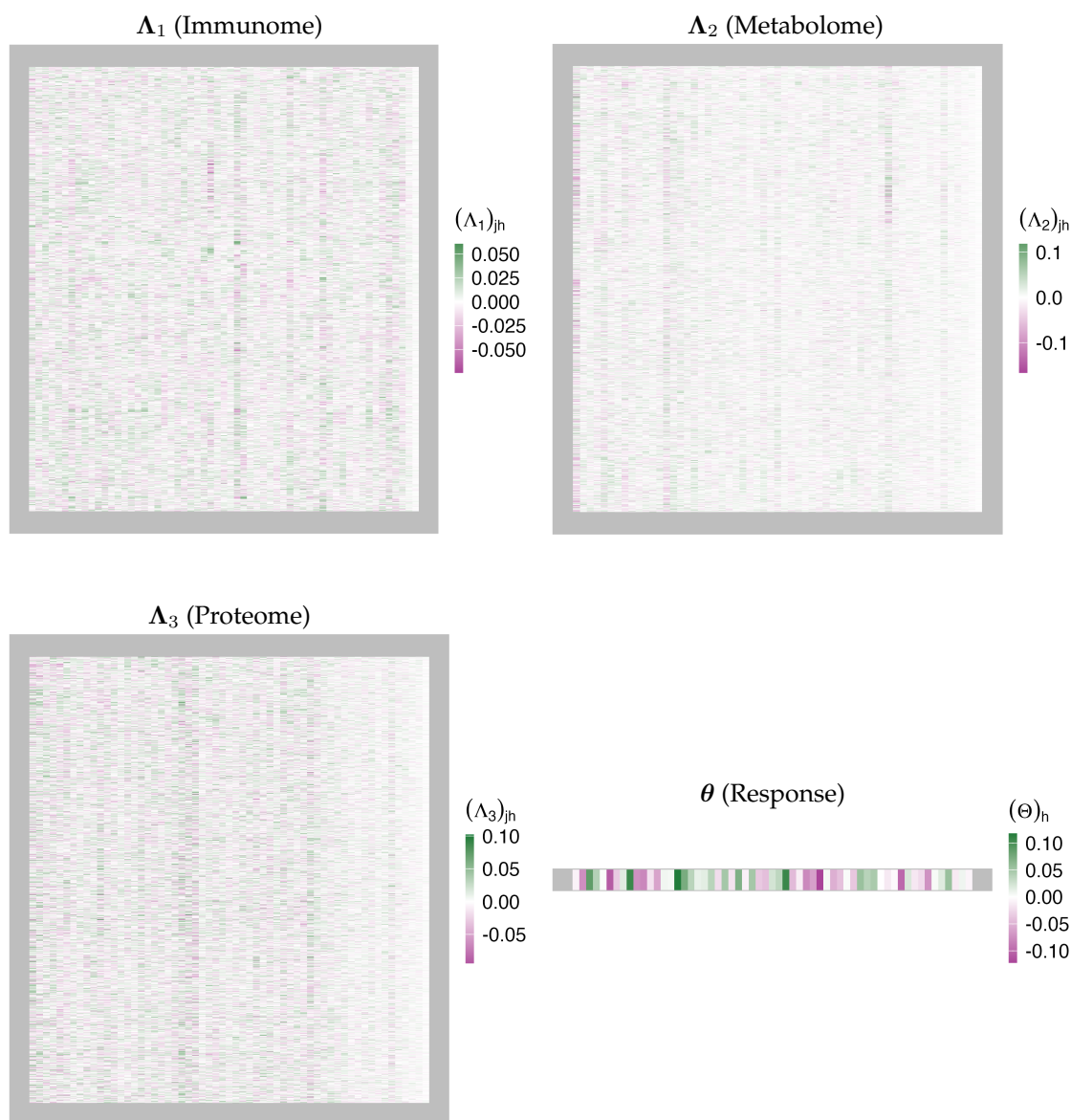


Figure 8: Posterior means of the shared-component loadings matrices, after post-processing via multiview Varimax.

References

- Albert, J. & Chib, S. (1993), ‘Bayesian analysis of binary and polychotomous response data’, *Journal of the American Statistical Association* **88**(422), 669–679.
- Argelaguet, R., Velten, B., Arnol, D., Dietrich, S., Zenz, T., Marioni, J. C., Buettner, F., Huber, W. & Stegle, O. (2018), ‘Multi-omics factor analysis — A framework for unsupervised integration of multi-omics data sets’, *Molecular Systems Biology* **14**(6), e8124.
- Bhattacharya, A. & Dunson, D. B. (2011), ‘Sparse Bayesian infinite factor models’, *Biometrika* **98**(2), 291–306.
- Bhattacharya, A., Pati, D., Pillai, N. S. & Dunson, D. B. (2015), ‘Dirichlet–Laplace priors for optimal shrinkage’, *Journal of the American Statistical Association* **110**(512), 1479–1490.

- Carvalho, C. M., Chang, J., Lucas, J. E., Nevins, J. R., Wang, Q. & West, M. (2008), 'High-dimensional sparse factor modeling: Applications in gene expression genomics', *Journal of the American Statistical Association* **103**(484), 1438–1456.
- Chandra, N. K., Canale, A. & Dunson, D. B. (2023), 'Escaping the curse of dimensionality in bayesian model-based clustering', *Journal of Machine Learning Research* **24**(144), 1–42.
- Chandra, N. K., Dunson, D. B. & Xu, J. (2023), 'Inferring covariance structure from multiple data sources via subspace factor analysis', *arXiv preprint arXiv:2305.04113*.
- Ding, D. Y., Li, S., Narasimhan, B. & Tibshirani, R. (2022), 'Cooperative learning for multiview analysis', *Proceedings of the National Academy of Sciences* **119**(38), e2202113119.
- Feldman, J. & Kowal, D. R. (2023), 'Nonparametric copula models for multivariate, mixed, and missing data', *arXiv preprint arXiv:2210.14988*.
- Ferrari, F. & Dunson, D. B. (2021), 'Bayesian factor analysis for inference on interactions', *Journal of the American Statistical Association* **116**(535), 1521–1532.
- Gavish, M. & Donoho, D. L. (2017), 'Optimal shrinkage of singular values', *IEEE Transactions on Information Theory* **63**(4), 2137–2152.
- Hahn, P. R., Mukherjee, S. & Carvalho, C. M. (2013), 'Partial factor modeling: Predictor-dependent shrinkage for linear regression', *Journal of the American Statistical Association* **108**(503), 999–1008.
- Hoff, P. D. (2007), 'Extending the rank likelihood for semiparametric copula estimation', *The Annals of Applied Statistics* **1**(1), 265–283.
- Ishwaran, H. & James, L. F. (2001), 'Gibbs sampling methods for stick-breaking priors', *Journal of the American statistical Association* **96**(453), 161–173.
- Kaiser, H. F. (1958), 'The varimax criterion for analytic rotation in factor analysis', *Psychometrika* **23**(3), 187–200.
- Klaassen, C. A., Wellner, J. A. et al. (1997), 'Efficient estimation in the bivariate normal copula model: normal margins are least favourable', *Bernoulli* **3**(1), 55–77.
- Lee, S. I. & Yoo, S. J. (2020), 'Multimodal deep learning for finance: Integrating and forecasting international stock markets', *The Journal of Supercomputing* **76**, 8294–8312.
- Legramanti, S., Durante, D. & Dunson, D. B. (2020), 'Bayesian cumulative shrinkage for infinite factorizations', *Biometrika* **107**(3), 745–752.
- Li, G. & Jung, S. (2017), 'Incorporating covariates into integrated factor analysis of multi-view data', *Biometrics* **73**(4), 1433–1442.
- Li, Q. & Li, L. (2022), 'Integrative factor regression and its inference for multimodal data analysis', *Journal of the American Statistical Association* **117**(540), 2207–2221.
- Li, R., Ma, F. & Gao, J. (2021), Integrating multimodal electronic health records for diagnosis prediction, in 'AMIA Annual Symposium Proceedings', Vol. 2021, American Medical Informatics Association, p. 726.
- Lock, E. F., Hoadley, K. A., Marron, J. S. & Nobel, A. B. (2013), 'Joint and individual variation explained (JIVE) for integrated analysis of multiple data types', *The Annals of Applied Statistics* **7**(1), 523 – 542.
- Mallick, H., Porwal, A., Saha, S., Basak, P., Svetnik, V. & Paul, E. (2024), 'An integrated Bayesian framework for multi-omics prediction and classification', *Statistics in Medicine* **43**(5), 983–1002.
- McNaboe, R., Beardslee, L., Kong, Y., Smith, B. N., Chen, I.-P., Posada-Quintero, H. F. & Chon, K. H. (2022), 'Design and validation of a multimodal wearable device for simultaneous collection of electrocardiogram, electromyogram, and electrodermal activity', *Sensors* **22**(22), 8851.
- Moran, K. R., Dunson, D. B., Wheeler, M. W. & Herring, A. H. (2021), 'Bayesian joint modeling of chemical structure and dose response curves', *The Annals of Applied Statistics* **15**(3), 1405 – 1430.
- Murray, J. S., Dunson, D. B., Carin, L. & Lucas, J. E. (2013), 'Bayesian gaussian copula factor models for mixed data', *Journal of the American Statistical Association* **108**(502), 656–665.
- Palzer, E. F., Wendt, C. H., Bowler, R. P., Hersh, C. P., Safo, S. E. & Lock, E. F. (2022), 'sjive: Supervised joint and individual variation explained', *Computational Statistics & Data Analysis* **175**, 107547.

- Park, T. & van Dyk, D. A. (2009), 'Partially collapsed gibbs samplers: Illustrations and applications', *Journal of Computational and Graphical Statistics* **18**(2), 283–305.
- Poworoznek, E., Ferrari, F. & Dunson, D. B. (2021), 'Efficiently resolving rotational ambiguity in bayesian matrix sampling with matching', *arXiv preprint arXiv:2107.13783*.
- Roberts, G. O. & Rosenthal, J. S. (2007), 'Coupling and ergodicity of adaptive markov chain monte carlo algorithms', *Journal of applied probability* **44**(2), 458–475.
- Roy, A., Lavine, I., Herring, A. H. & Dunson, D. B. (2021), 'Perturbed factor analysis: Accounting for group differences in exposure profiles', *The Annals of Applied Statistics* **15**(3), 1386 – 1404.
- Samorodnitsky, S., Wendt, C. H. & Lock, E. F. (2024), 'Bayesian simultaneous factorization and prediction using multi-omic data', *Computational Statistics & Data Analysis* **198**(1), In Press.
- Schiavon, L., Canale, A. & Dunson, D. B. (2022), 'Generalized infinite factorization models', *Biometrika* **109**(3), 817–835.
- Sklar, A. (1959), 'Fonctions de repartition an dimensions et leurs marges', *Publications de l'Institut de statistique de l'Université de Paris* **8**, 229–231.
- Stelzer, I. A., Ghaemi, M. S., Han, X., Ando, K., Hédou, J. J., Feyaerts, D., Peterson, L. S., Rumer, K. K., Tsai, E. S., Ganio, E. A., Gaudillière, D. K., Tsai, A. S., Choisy, B., Gaigne, L. P., Verdonk, F., Jacobsen, D., Gavasso, S., Traber, G. M., Ellenberger, M., Stanley, N., Becker, M., Culos, A., Fallahzadeh, R., Wong, R. J., Darmstadt, G. L., Druzin, M. L., Winn, V. D., Gibbs, R. S., Ling, X. B., Sylvester, K., Carvalho, B., Snyder, M. P., Shaw, G. M., Stevenson, D. K., Contrepolis, K., Angst, M. S., Aghaeepour, N. & Gaudillière, B. (2021), 'Integrated trajectories of the maternal metabolome, proteome, and immunome predict labor onset', *Science Translational Medicine* **13**(592), eabd9898.
- Vito, R. D., Bellio, R., Trippa, L. & Parmigiani, G. (2021), 'Bayesian multistudy factor analysis for high-throughput biological data', *The Annals of Applied Statistics* **15**(4), 1723 – 1741.

Appendix A Simulated data: further results

In the present section, we provide further evidence of the performances of the proposed methodology on the simulated data. We begin by complementing the results from Figure 1 with the associated uncertainty quantification. Figure A1 shows that `IntegLearn` and `BSFP` incur severe undercoverage, while `JAFAR` slightly overestimates the width of the intervals.

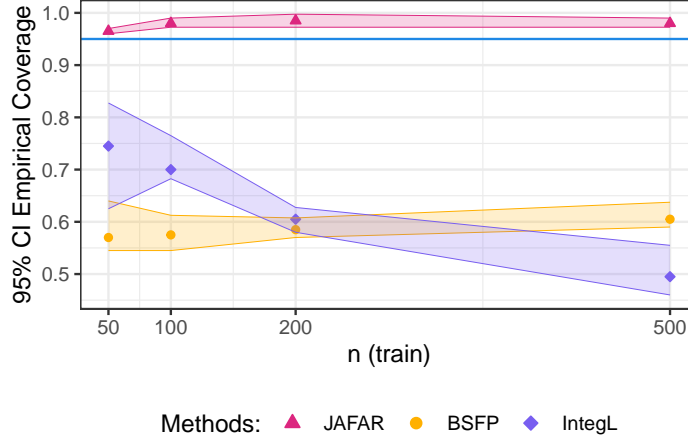


Figure A1: Empirical coverage of the 95% predictive intervals on the test sets of simulated data. The x-axis reports increasing size of the train set. The interior points and band edges correspond to the quartiles over 10 independent replicates for fixed dimensions. The horizontal blue corresponds to the correct coverage.

To provide more insight into feature structure learning, we further break down the results for one of the replicates for $n = 500$ from Section 3. We focus first on induced coefficients $\beta_m = \beta_m(\Lambda_m, \Gamma_m, \sigma_m^2, \theta)$ in the induced linear regression $\mathbb{E}[y_i | \{\mathbf{X}_{mi}\}_{m=1}^M] = \sum_{m=1}^M \beta_m \mathbf{X}_{mi}$. Recall that we set up the simulations so that half of the features of each view do not load directly to response-related factors. This translates into small values of the associated regression coefficients, while collinearity with other features prevents them from being exactly zero. The results in Figure A2 show the potential of both factor models to distinguish which features are more relevant for predictive purposes.

However, `JAFAR` does so without being affected by a general overshrinking towards zero, that characterizes `BSFP`. Conversely, the inconsistency between `CoopLearn` and the true regression coefficients is expected, due to the strong collinearity between the predictors. The underlying elastic net notoriously tends to select one non-zero coefficient for each group of correlated variables.

In Figure A3, we report the correlation matrices for each view, conditioned on all the others. For the two-factor models, we obtained the latter from the empirical correlations of draws from $p(\mathbf{X}_m | \{\mathbf{X}_{m'}\}_{m' \neq m})$. This shows that the posterior samples of `BSFP` partially correct for the dysfunctional scale set the prior variances r_o and r_m . Despite this, `JAFAR` still achieves superior predictors reconstruction.

Appendix B Gibbs Sampler for JAFAR under D-CUSP

In the current Section, we report the details of the implementation of the partially collapsed Gibbs sampler for the linear version of `JAFAR`, under the proposed D-CUSP prior for the shared loadings matrix Λ_m and response coefficients θ . As before, let us define $\mathbf{Z}_m = [\mathbf{z}_{m1}^\top, \dots, \mathbf{z}_{mn}^\top]^\top \in \mathbb{R}^{n \times p_m}$ for every $m = 1, \dots, M$. We presented the algorithm in terms of the transformed features $\mathbf{z}_{mij} = \Phi^{-1}(\hat{F}_{mj}(\mathbf{x}_{mij}))$ within the Gaussian copula factor model formulation. Nonetheless, the same structure holds in the absence of the copula layer, by simply replacing \mathbf{z}_{mij} with \mathbf{x}_{mij} .

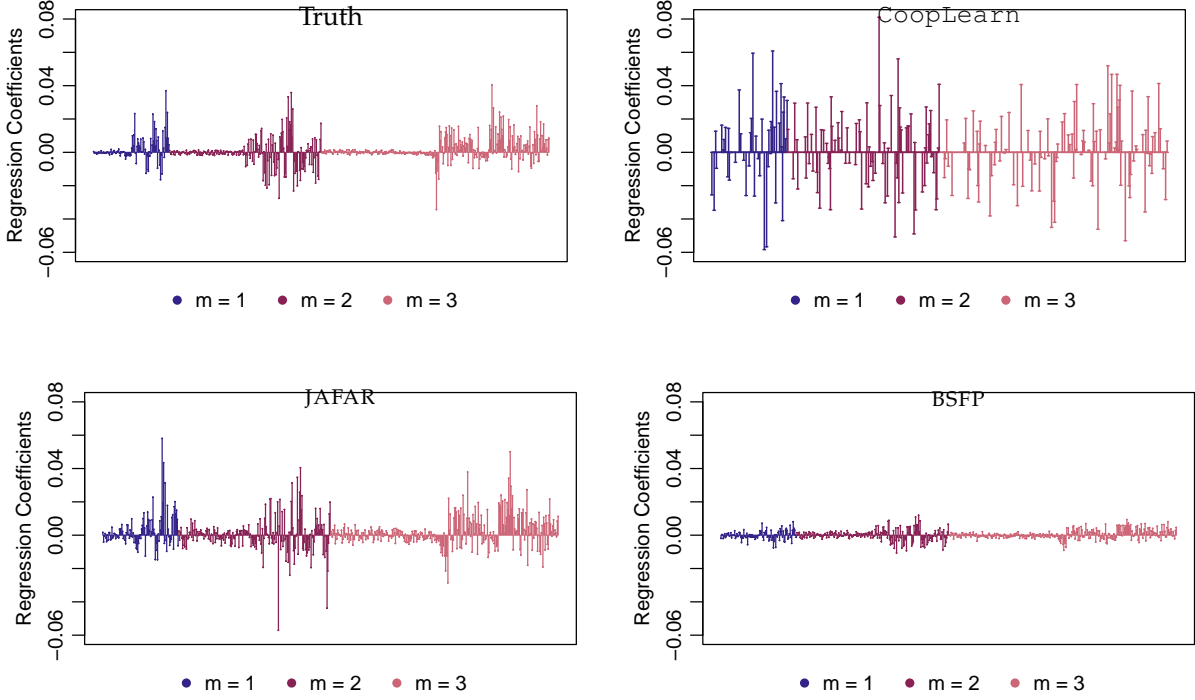


Figure A2: Regression coefficients in one replicate of the considered simulated data for $n = 500$. For the factor models considered, these corresponded to the Monte Carlo average of the induced coefficients. Both JAFAR and BSFP manage to distinguish between weakly and strongly predictive features. JAFAR further prevents underestimation of the relevant ones, leading to better prediction power. The elastic net underlying *CoopL* tends to select one non-zero coefficient per group of correlated variables.

Algorithm A1: One cycle of the partially collapsed Gibbs sampler for JAFAR with the D-CUSP prior on the shared loadings

1. sample $[\mu_y, \boldsymbol{\theta}]$ from $\mathcal{N}_{1+K}(\mathbf{V}_\theta \mathbf{u}_\theta, \mathbf{V}_\theta)$, where

$$\begin{cases} \mathbf{V}_\theta = (\text{diag}([v_y^{-2}, \{\chi_h^{-2}\}_{h=1}^K])^{-1} + \sigma_y^{-2}[\mathbf{1}_n, \boldsymbol{\eta}]^\top [\mathbf{1}_n, \boldsymbol{\eta}])^{-1} \\ \mathbf{u}_\theta = \sigma_y^{-2}[\mathbf{1}_n, \boldsymbol{\eta}]^\top \mathbf{y} \end{cases}$$
2. for $m = 1, \dots, M$:
 - for $j = 1, \dots, p_m$:
 - sample $[\boldsymbol{\mu}_{mj}, \boldsymbol{\Lambda}_{mj\bullet}, \boldsymbol{\Gamma}_{mj\bullet}]$ from $\mathcal{N}_{1+K+K_m}(\mathbf{V}_{mj} \mathbf{u}_{mj}, \mathbf{V}_{mj})$, where

$$\begin{cases} \mathbf{V}_{mj} = (\text{diag}([v_m^{-2}, \{\chi_{mh}^{-2}\}_{h=1}^K, \{\tau_{mh}^{-2}\}_{h=1}^{K_m}])^{-1} + \sigma_{mj}^{-2}[\mathbf{1}_n, \boldsymbol{\eta}, \boldsymbol{\phi}_m]^\top [\mathbf{1}_n, \boldsymbol{\eta}, \boldsymbol{\phi}_m])^{-1} \\ \mathbf{u}_{mj} = \sigma_{mj}^{-2}[\mathbf{1}_n, \boldsymbol{\eta}, \boldsymbol{\phi}_m]^\top \mathbf{Z}_{m\bullet j} \end{cases}$$
3. sample σ_y^2 from $\text{InvGa}(a^{(y)} + 0.5n, b^{(y)} + 0.5 \sum ((\mathbf{y} - \mathbf{1}_n \mu_y - \boldsymbol{\eta} \boldsymbol{\theta})^2))$
 - for $m = 1, \dots, M$:
 - for $j = 1, \dots, p_m$:
 - sample σ_{mj}^2 from $\text{InvGa}(a^{(m)} + 0.5n, b^{(m)} + 0.5d_{mj})$, where

$$d_{mj} = \sum ((\mathbf{Z}_{m\bullet j} - \mathbf{1}_n \boldsymbol{\mu}_{mj} - \boldsymbol{\eta} \boldsymbol{\Lambda}_{mj\bullet} - \boldsymbol{\phi}_m \boldsymbol{\Gamma}_{mj\bullet})^2)$$
4. for $i = 1, \dots, n$:
 - sample $\boldsymbol{\eta}_i$ from $\mathcal{N}_K(\mathbf{V} \mathbf{u}_i, \mathbf{V})$, where

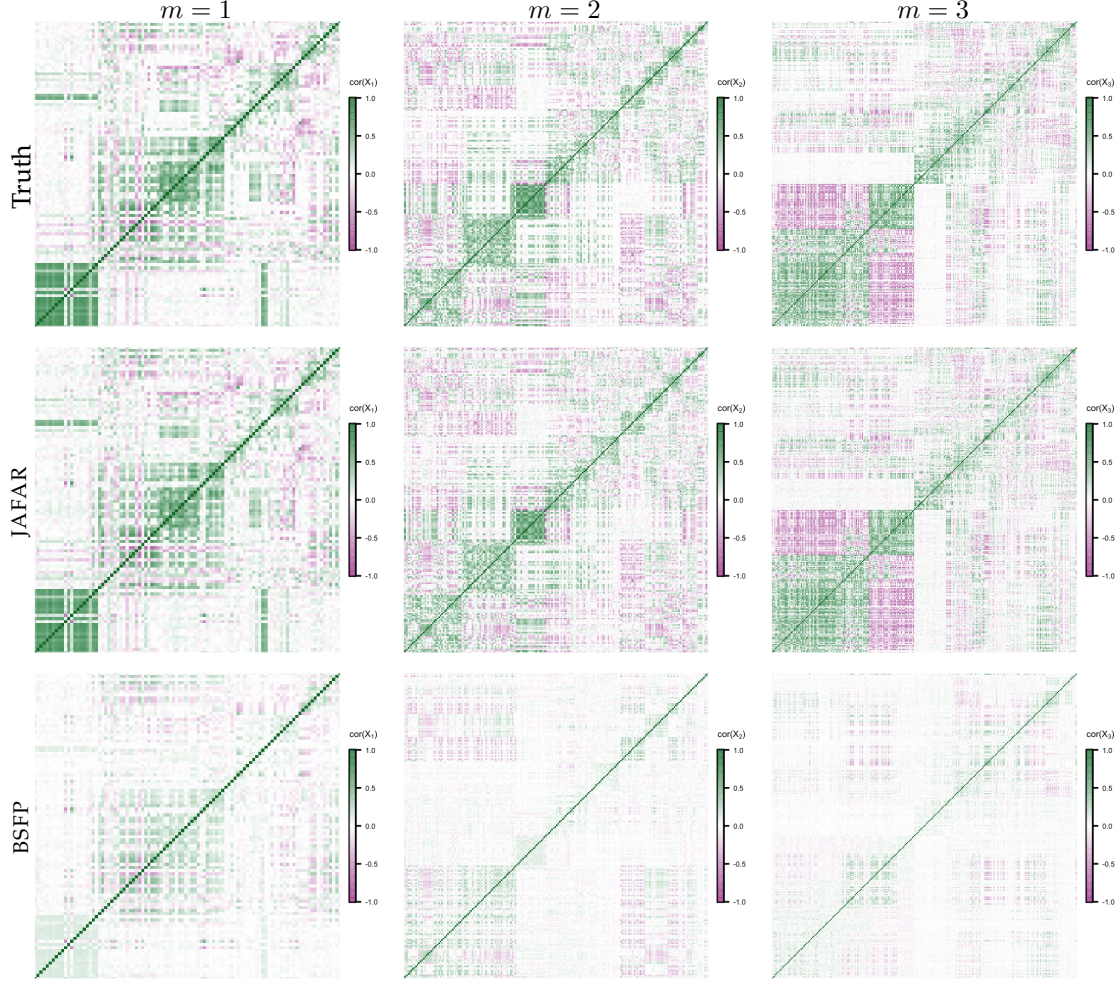


Figure A3: Within-view correlation matrices in one replicate of the considered simulated data for $n = 500$. The first row reports the true correlations for each view, conditioned on the remaining ones. The realistic block structure is obtained via our original simulation setup for the loading matrices, detailed in Appendix D. For JAFAR and BSFP, we considered here the average correlations matrix $\frac{1}{n_{\text{MCMC}}} \sum_{t=1}^{n_{\text{MCMC}}} \text{cor}(\mathbf{X}_m^{(t)})$ over MCMC samples from the full conditional $\mathbf{X}_m^{(t)} \sim p(\mathbf{X}_m | \{\mathbf{X}_{m'}\}_{m' \neq m})$ of the corresponding view given all the others (response excluded).

$$\begin{cases} \mathbf{V} = \left(\mathbf{I}_K + \sigma_y^{-2} \boldsymbol{\theta} \boldsymbol{\theta}^\top + \sum_{m=1}^M \boldsymbol{\Lambda}_m^\top (\boldsymbol{\Gamma}_m \boldsymbol{\Gamma}_m^\top + \text{diag}(\boldsymbol{\sigma}_m^2))^{-1} \boldsymbol{\Lambda}_m \right)^{-1} \\ \mathbf{u}_i = \sigma_y^{-2} \boldsymbol{\theta} (\mathbf{y}_i - \mu_y) + \sum_{m=1}^M \boldsymbol{\Lambda}_m^\top (\boldsymbol{\Gamma}_m \boldsymbol{\Gamma}_m^\top + \text{diag}(\boldsymbol{\sigma}_m^2))^{-1} (\mathbf{Z}_{mi\cdot} - \boldsymbol{\mu}_m) \end{cases}$$

5. for $i = 1, \dots, n$:
 - for $m = 1, \dots, M$:
 - sample ϕ_{mi} from $\mathcal{N}_{K_m}(\mathbf{V}_m \mathbf{u}_{mi}, \mathbf{V}_m)$, where

$$\begin{cases} \mathbf{V}_m = (\mathbf{I}_{K_m} + \boldsymbol{\Gamma}_m^\top \text{diag}(\boldsymbol{\sigma}_m^{-2}) \boldsymbol{\Gamma}_m)^{-1} \\ \mathbf{u}_{mi} = \boldsymbol{\Gamma}_m^\top \text{diag}(\boldsymbol{\sigma}_m^{-2}) (\mathbf{Z}_{mi\cdot} - \boldsymbol{\mu}_m - \boldsymbol{\Lambda}_m \boldsymbol{\eta}_i) \end{cases}$$
6. for $h = 1, \dots, K$:
 - sample the binary indicator δ_h according to equation (B1)
 - for $m = 1, \dots, M$:
 - for $h = 1, \dots, K$:
 - sample the categorical indicator δ_{mh} according to equation (B1)

- for $h = 1, \dots, K_m$:
 sample the categorical indicator ζ_{mh} according to equation (B1)
7. sample ξ from $\mathcal{B}e(a^{(\xi)} + \sum_{h=1}^K \mathbb{1}_{(\delta_h=0)}, b^{(\xi)} + \sum_{h=1}^K \mathbb{1}_{(\delta_h=1)})$
 for $m = 1, \dots, M$:
 for $h = 1, \dots, K - 1$:
 sample ρ_{mh} from $\mathcal{B}e(1 + \sum_{l=1}^K \mathbb{1}_{(\delta_l=h)}, \alpha_m^{(\Lambda)} + \sum_{l=1}^K \mathbb{1}_{(\delta_l>h)})$
 for $h = 1, \dots, K_m - 1$:
 sample ν_{mh} from $\mathcal{B}e(1 + \sum_{l=1}^K \mathbb{1}_{(\delta_l=h)}, \alpha_m^{(\Gamma)} + \sum_{l=1}^K \mathbb{1}_{(\delta_l>h)})$
8. for $h = 1, \dots, K$:
 if $(\delta_h = 1$ and $\max_m \delta_{mh} > h)$ sample χ_h^2 from
 $\mathcal{I}nv\mathcal{G}a(a^{(\theta)} + 0.5, b^{(\theta)} + 0.5 \theta_h^2)$ else set $\chi_h^2 = \chi_\infty^2$
 for $m = 1, \dots, M$:
 for $h = 1, \dots, K$:
 if $(\delta_{mh} > h$ and $(\delta_h = 1$ or $\max_{m' \neq m} \delta_{m'h} > h))$ sample χ_{mh}^2 from
 $\mathcal{I}nv\mathcal{G}a(a_m^{(\Lambda)} + 0.5 p_m, b_m^{(\Lambda)} + 0.5 \sum_{j=1}^{p_m} \Lambda_{mj}^2)$ else set $\chi_{mh}^2 = \chi_{m\infty}^2$
 for $h = 1, \dots, K_m$:
 if $\zeta_{mh} > h$ sample τ_{mh}^2 from $\mathcal{I}nv\mathcal{G}a(a_m^{(\Gamma)} + 0.5 p_m, b_m^{(\Gamma)} + 0.5 \sum_{j=1}^{p_m} \Gamma_{mj}^2)$
 else set $\tau_{mh}^2 = \tau_{m\infty}^2$

To complete the specification of the sampler, we provide here the details for the computation of the probability mass functions of the latent indicators from the CUSP constructions. In particular, we employ the same strategy of original contribution by Legramanti et al. (2020), sampling all latent indicators from the corresponding collapsed full conditionals after the marginalization of the loadings variances χ_h^2 , χ_{mh}^2 and τ_{mh}^2

$$\begin{aligned} \mathbb{P}[\delta_h = s_h \mid \{\delta_{mh} = s_{mh}\}_m, \boldsymbol{\theta}_h, \{\Lambda_{m \bullet h}\}_m, \xi] &= (1 - \xi)^{s_h} \cdot \xi^{s_h} \cdot \\ &\cdot f(\boldsymbol{\theta}_h \mid \delta_h = s_h, \{\delta_{mh} = s_{mh}\}_m) \prod_{m=1}^M f(\Lambda_{m \bullet h} \mid \delta_h = s_h, \{\delta_{m'h} = s_{m'h}\}_{m'}) \\ \mathbb{P}[\delta_{mh} = s_{mh} \mid \delta_h = s_h, \{\delta_{m'h} = s_{m'h}\}_{m' \neq m}, \boldsymbol{\theta}_h, \{\Lambda_{m' \bullet h}\}_{m'}, \{\rho_{m' \bullet}\}_{m'}] &= \xi_{m s_{mh}} \cdot \\ &\cdot f(\boldsymbol{\theta}_h \mid \delta_h = s_h, \{\delta_{m'h} = s_{m'h}\}_{m'}) \prod_{m'=1}^M f(\Lambda_{m' \bullet h} \mid \delta_h = s_h, \{\delta_{m''h} = s_{m''h}\}_{m''}) \\ \mathbb{P}[\zeta_{mh} = \ell_{mh} \mid \mathbf{\Gamma}_{m \bullet h}, \nu_{m \bullet}] &= \omega_{m \ell_{mh}} \cdot f(\mathbf{\Gamma}_{m \bullet h} \mid \zeta_{mh} = \ell_{mh}), \end{aligned} \quad (\text{B1})$$

where $s_h \in \{0, 1\}$, $s_{mh} \in \{1, \dots, K\}$ for each $m = 1, \dots, M$ and $h = 1, \dots, K$, while $\ell_{mh} \in \{1, \dots, K_m\}$ for each $m = 1, \dots, M$ and $h = 1, \dots, K_m$. Recall that $\xi_{m s_{mh}} = \rho_{mh} \prod_{l=1}^{h-1} (1 - \rho_{ml})$ and $\omega_{m \ell_{mh}} = \nu_{mh} \prod_{l=1}^{\ell_{mh}-1} (1 - \nu_{ml})$. Similarly to Legramanti et al. (2020), the required loadings conditional pdf appearing in equation (B1) take the form

$$f(\mathbf{\Gamma}_{m \bullet h} \mid \zeta_{mh} = \ell_{mh}) = \begin{cases} t_{p_m, 2 a_m^{(\Gamma)}}(\mathbf{\Gamma}_{m \bullet h}; \mathbf{0}_{p_m}, (b_m^{(\Gamma)} / a_m^{(\Gamma)}) \mathbf{I}_{p_m}) & \text{if } \ell_{mh} > h \\ \phi_{p_m}(\mathbf{\Gamma}_{m \bullet h}; \mathbf{0}_{p_m}, \tau_{m\infty}^2 \mathbf{I}_{p_m}) & \text{otherwise} \end{cases}$$

and

$$\begin{aligned} f(\boldsymbol{\theta}_h \mid \delta_h = s_h, \{\delta_{mh} = s_{mh}\}_{m=1}^M) &= \\ &\begin{cases} t_{2 a^{(\theta)}}(\boldsymbol{\theta}_h; 0, b^{(\theta)} / a^{(\theta)}) & \text{if } (s_h = 1 \text{ and } \max_m s_{mh} > h) \\ \phi(\boldsymbol{\theta}_h; 0, \chi_\infty^2) & \text{otherwise} \end{cases} \\ f(\Lambda_{m \bullet h} \mid \delta_h = s_h, \{\delta_{m'h} = s_{m'h}\}_{m'=1}^M) &= \\ &\begin{cases} t_{p_m, 2 a_m^{(\Lambda)}}(\Lambda_{m \bullet h}; \mathbf{0}_{p_m}, (b_m^{(\Lambda)} / a_m^{(\Lambda)}) \mathbf{I}_{p_m}) & \text{if } (s_{mh} > h \text{ and } (s_h = 1 \text{ or } \max_{m' \neq m} s_{m'h} > h)) \\ \phi_{p_m}(\Lambda_{m \bullet h}; \mathbf{0}_{p_m}, \chi_{m\infty}^2 \mathbf{I}_{p_m}) & \text{otherwise,} \end{cases} \end{aligned}$$

where $t_{p, \kappa}(\cdot; \mathbf{m}, \mathbf{C})$ and $\phi_p(\cdot; \mathbf{m}, \mathbf{C})$ denotes the pdf of a p -variate Student- t and normal distributions, respectively, where $\kappa > 1$ stands for the degrees of freedom, \mathbf{m} is a location vector and \mathbf{C} is a scale matrix.

As mentioned before, we consider a truncated version of the CUSP and D-CUSP priors, entailing finite upper bound K and $\{K_m\}_m$ to the number of shared and view-specific factors respectively. To preserve flexibility, we tune them adaptively according to Algorithm B2.

Algorithm B2: Adaption of the number of shared and view-specific factors at the t^{th} iteration of the Gibbs sampler.

$u_t \sim \mathcal{U}(0, 1)$

if $t \geq t_{\text{adapt}}$ and $u_t < \exp(d_0 + d_1 t)$ **then**

$K^* = K - \sum_{h=1}^K \mathbb{1}_{(\delta_h=1)} + \sum_{m=1}^M \mathbb{1}_{(\delta_{mh}>h)} \leq 1$

if $K^* < K - 1$ **then**

set $K = K^* + 1$. Drop the inactive columns in $\{\Lambda_m\}_m$ and θ , along with the associated elements in η, χ, χ_m and ξ_m . Add an inactive shared factor, sampling from the spike the corresponding loadings and from the prior all other involved quantities

else

set $K = K + 1$. Add an inactive shared factor, sampling from the spike the corresponding loadings and from the prior all other involved quantities

for $m = 1, \dots, M$ **do**

$K_m^* = K_m - \sum_{h=1}^{K_m} \mathbb{1}_{(\zeta_{mh} \leq h)}$

if $K_m^* < K_m - 1$ **then**

set $K_m = K_m^* + 1$. Drop the inactive columns in $\{\Gamma_m\}_m$, along with the associated elements in ϕ_m, τ_m and ω_m . Add an inactive specific factor for the m^{th} view, sampling from the spike the corresponding loadings and from the prior all other involved quantities

else

set $K_m = K_m + 1$. Add an inactive specific factor for the m^{th} view, sampling from the spike the corresponding loadings and from the prior all other involved quantities

Appendix C Further modeling extensions; non-linear an discrete responses

JAFAR can be easily generalized to account for deviations from normality and linearity in the response, other than binary and count y . In the current section, we present different ways to achieve this, adapting the proposed D-CUSP prior. For the sake of completeness, we note that higher flexibility could be achieved also considering alternative approaches, beyond those reported below. For instance, recent contributions in factor models have shown the benefit of assuming a mixture of normals as prior distribution for the latent factors (Chandra, Canale & Dunson 2023).

C.0.1 Non-linear response modeling: interactions & splines

The specific structure of JAFAR allows the introduction of a more flexible dependence of y_i on η_i with minimal computational drawbacks. While such non-linearity typically breaks down conditionally conjugate updates for the shared factor, all remaining components of the model are unaffected in this respect. Accordingly, the Gibbs sampler from the previous Section remains unchanged, except for step 4. Analogous extensions of BSFP would instead require non-conjugate updates even for the view-specific factors, which would be highly detrimental to good mixing of the MCMC chain.

Interactions among latent factors

Aside from multiview integration frameworks, Ferrari & Dunson (2021) recently generalized Bayesian latent factor regression to accommodate interactions among the latent variables in the response component

$$y_i = \mu_y + \beta^\top \mathbf{r}_i + \theta^\top \eta_i + \eta_i^\top \Omega \eta_i + e_i,$$

where Ω is a $K \times K$ symmetric matrix. Other than providing theory on model misspecification and consistency, the authors showed that the above formulation induces a quadratic regression of y_i on the transformed concatenated features \mathbf{z}_i

$$\mathbb{E}[y_i | \mathbf{z}_i] = \mu_y + (\boldsymbol{\theta}^\top \mathbf{A}) \mathbf{z}_i + \mathbf{z}_i^\top (\mathbf{A}^\top \Omega \mathbf{A}) \mathbf{z}_i + \text{tr}(\Omega \mathbf{V}), \quad (\text{C1})$$

where as before $\mathbf{V} = (\mathbf{A}^\top \mathbf{D}^{-1} \mathbf{A} + \mathbf{I}_K)^{-1}$ and $\mathbf{A} = \mathbf{V} \mathbf{A}^\top \mathbf{D}^{-1}$. The same results directly apply to JAFAR as well, as its composite nature is reflected solely in the structure of such matrices. In fact, recalling that here $\mathbf{A} = [\mathbf{A}_1^\top, \dots, \mathbf{A}_M^\top]^\top$, it is easy to show that now $\mathbf{D} = \text{block-diag}(\{\mathbf{D}_m\}_{m=1}^M)$, where $\mathbf{D}_m = \Gamma_m \Gamma_m^\top + \text{diag}(\boldsymbol{\sigma}_m^2)$ represent the marginal covariance structure of the m^{th} view conditioned on the shared factors $\boldsymbol{\eta}_i$, after marginalization of the specific ones ϕ_{mi} . Accordingly, the additive structure of JAFAR allows once again to cut down computations, as the bottleneck evaluation of $\mathbf{A}^\top \mathbf{D}^{-1} \mathbf{A} = \sum_{m=1}^M \mathbf{A}_m^\top \mathbf{D}_m^{-1} \mathbf{A}_m$ can be done at $\mathcal{O}(\sum_{m=1}^M p_m (K + K_m)^2)$ cost rather than $\mathcal{O}((\sum_{m=1}^M p_m)(K + \sum_{m=1}^M K_m)^2)$. Notice that, as in the original contribution by Ferrari & Dunson (2021), we could define Ω as a diagonal matrix and we would still estimate pairwise interactions between the regressors. In such case, the D-CUSP prior would unfold also each element Ω_{hh} , for instance setting

$$\Omega_{hh} \sim \mathcal{N}(0, \gamma_h^2) \quad \gamma_h^2 \sim \psi_h \text{InvGa}(a^{(\Omega)}, b^{(\Omega)}) + (1 - \psi_h) \delta_{\gamma_\infty^2}.$$

Through appropriate modifications of the factor modeling structure, the same rationale can be extended to accommodate higher-order interactions, or interactions among the shared factors $\boldsymbol{\eta}_i$ and the clinical covariates \mathbf{r}_i . Conversely, we highlight that the standard version of JAFAR would induce a linear regression of y_i on the feature data, which boils down to dropping the last two terms on the right of equation (C1). The inclusion of pairwise interactions among the factors in the response component breaks conditional conjugacy for the shared factors. To address this issue, the authors suggested updating $\boldsymbol{\eta}_i$ using the Metropolis-adjusted Langevin algorithm (MALA) (Grenander and Miller 1994; Roberts and Tweedie 1996). In this respect, we highlight that a similar quadratic extension of BSFP would require updating $(M + 1) \cdot n$ vectors, of dimensions $\{K, K_1, \dots, K_M\}$, while JAFAR allows to reduce this major computational bottleneck to n vectors of dimensions K .

Bayesian B-splines

To allow for higher flexibility of the response surface, one possibility is to model the continuous outcome with a nonparametric function of the latent variables. As this would however create several computational challenges, we instead focus on modeling $f(\cdot)$ using Bayesian B-splines of degree D :

$$f(\boldsymbol{\eta}_i) = \sum_{h=1}^K \sum_{d=1}^{D+2} \Theta_{hd} b_d(\boldsymbol{\eta}_{ih}),$$

where $b_d(\cdot)$, for $d = 1, \dots, D + 2$, denotes the d^{th} function in a B-spline basis of degree D with natural boundary constraints. Let $\varrho = (\varrho_1, \dots, \varrho_D)$ be the boundary knots, then $b_1(\cdot)$ and $b_{D+2}(\cdot)$ are linear functions in the intervals $[-\infty, \varrho_1]$ and $[\varrho_D, +\infty]$, respectively. In particular, we assume cubic splines (i.e. $D = 3$), but the model can be easily estimated for higher-order splines. As before, the update of the shared factors needs to be performed via a Metropolis-within-Gibbs step, without modifying the other steps of the sampler. In such a case, the D-CUSP can be extended simply by setting

$$\Theta_{hd} \sim \mathcal{N}(0, \chi_h^2) \quad \chi_h^2 \sim \psi_h \text{InvGa}(a^{(\Theta)}, b^{(\Theta)}) + (1 - \psi_h) \delta_{\chi_\infty^2}.$$

C.0.2 Categorical and count outcomes: GLMs factor regression

The JAFAR construction can be modified to accommodate for non-continuous outcomes y_i as well, while still allowing for deviation from linearity assumptions via the quadratic regression setting presented above. For instance, binary responses can be trivially modeled via a probit link $y_i \sim \text{Ber}(\varphi_i)$ with $\varphi_i = \Phi(\boldsymbol{\theta}^\top \boldsymbol{\eta}_i + \boldsymbol{\eta}_i^\top \Omega \boldsymbol{\eta}_i)$. Except for the shared factors $\boldsymbol{\eta}_i$, conditional conjugacy is preserved by appealing to a well-known data augmentation strategy in terms of latent variable $q_i \in \mathbb{R}$ (Albert & Chib 1993), such that $y_i = 1$ if $q_i > 0$ and $y_i = 0$ if $q_i \leq 0$.

More generally, in the remainder of this Section, we show how to extend the same rationale to generalized linear models (GLM) with logarithmic link and responses in the exponential families. In doing so, we also compute expressions for induced main and interaction effects, allowing for a straightforward interpretation of the associated coefficients.

Factor regression with count data

In GLMs under logarithmic link, the logarithmic function is used to relate the linear predictor $\beta^\top \mathbf{r}_i$ to the conditional expectation of y_i given the covariates \mathbf{r}_i , such that $\log(\mathbb{E}[y_i|\mathbf{r}_i]) = \beta^\top \mathbf{r}_i$. Two renowned GLMs for count data are the Poisson and the Negative-Binomial models. Defining φ_i as the mean parameter for the i^{th} observation $\varphi_i = \mathbb{E}[y_i|\mathbf{r}_i] = e^{\beta^\top \mathbf{r}_i}$, such two alternatives correspond to $(y_i|\mathbf{r}_i) \sim \text{Poisson}(\varphi_i)$ and $(y_i|\mathbf{r}_i) \sim \text{NegBin}(\kappa/(\varphi_i + \kappa), \kappa)$, for some $\kappa \in [0, 1]$. A main limitation of the Poisson distribution is the fact that the mean and variance are equal, which motivates the use of negative-binomial regression to deal with over-dispersed count data. In both scenarios, we can integrate the GLM formulation in the quadratic latent factor structure presented above

$$\log(\mathbb{E}[y_i|\boldsymbol{\eta}_i]) = \boldsymbol{\theta}^\top \boldsymbol{\eta}_i + \boldsymbol{\eta}_i^\top \boldsymbol{\Omega} \boldsymbol{\eta}_i$$

Accordingly, it is easy to show the following.

Proposition 1 *Marginalizing out all latent factors in the quadratic GLM extension of JAFAR, both shared and view-specific ones, it holds that*

$$\mathbb{E}[y_i|\mathbf{z}_i] = \sqrt{|\mathbf{V}'|/|\mathbf{V}|} \exp\left(\frac{1}{2}\boldsymbol{\theta}^\top \mathbf{V}' \boldsymbol{\theta} + \boldsymbol{\theta}_X^\top \mathbf{z}_i + \mathbf{z}_i^\top \boldsymbol{\Omega}_X \mathbf{z}_i\right)$$

where $\boldsymbol{\theta}_X^\top = \boldsymbol{\theta}^\top (\mathbf{I}_K - 2\mathbf{V}\boldsymbol{\Omega})^{-1} \mathbf{A}$, $\boldsymbol{\Omega}_X = \frac{1}{2} \mathbf{A}^\top \mathbf{V}^{-1} ((\mathbf{I}_K - 2\mathbf{V}\boldsymbol{\Omega})^{-1} - \mathbf{I}_K) \mathbf{A}$ and $\mathbf{V}' = (\mathbf{V}^{-1} - 2\boldsymbol{\Omega})^{-1}$. As before, $\mathbf{V} = (\mathbf{A}^\top \mathbf{D}^{-1} \mathbf{A} + \mathbf{I}_K)^{-1}$ and $\mathbf{A} = \mathbf{V} \mathbf{A}^\top \mathbf{D}^{-1}$ comes for the full-conditional posterior of the shared factors $\boldsymbol{\eta}_i | \mathbf{z}_i \sim \mathcal{N}_K(\mathbf{A} \mathbf{z}_i, \mathbf{V})$, after marginalization of the view-specific factors.

This allows us to estimate quadratic effects with high-dimensional correlated predictors in regression settings with count data. Similarly to what seen before, the composite structure of JAFAR affects solely the bottleneck computation of the massive matrix $\mathbf{A}^\top \mathbf{D}^{-1} \mathbf{A}$, allowing to substantially reduce the associated computational cost by conveniently decomposing it.

Exponential family responses

We consider here an even more general scenario requiring only that the outcome distribution belongs to the exponential family

$$p(y_i|\varsigma_i) = \exp(\varsigma_i \cdot T(y_i) - U(\varsigma_i)),$$

where ς_i is the univariate natural parameter and $T(y_i)$ is a sufficient statistic. Accordingly, we generalize Gaussian linear factor models and set $\varsigma_i = \boldsymbol{\theta}^\top \boldsymbol{\eta}_i + \boldsymbol{\eta}_i^\top \boldsymbol{\Omega} \boldsymbol{\eta}_i$. As before, $\varphi_i = \mathbb{E}[y_i|\boldsymbol{\eta}_i] = g^{-1}(\boldsymbol{\theta}^\top \boldsymbol{\eta}_i + \boldsymbol{\eta}_i^\top \boldsymbol{\Omega} \boldsymbol{\eta}_i)$, where $g(\cdot)$ is a model-specific link function. Our goal is to compute the expectation of y_i given \mathbf{z}_i after integrating out all latent factors

$$\begin{aligned} \mathbb{E}[y_i|\mathbf{z}_i] &= \mathbb{E}[\mathbb{E}[y_i|\boldsymbol{\eta}_i|\mathbf{z}_i]] = \mathbb{E}[g^{-1}(\boldsymbol{\theta}^\top \boldsymbol{\eta}_i + \boldsymbol{\eta}_i^\top \boldsymbol{\Omega} \boldsymbol{\eta}_i)|\mathbf{z}_i] \\ &= \int g^{-1}(\boldsymbol{\theta}^\top \boldsymbol{\eta}_i + \boldsymbol{\eta}_i^\top \boldsymbol{\Omega} \boldsymbol{\eta}_i) p(\boldsymbol{\eta}_i|\mathbf{z}_i) d\boldsymbol{\eta}_i. \end{aligned}$$

In general, this represents the expectation of the natural parameter conditional on \mathbf{z}_i for any distribution within the exponential family. Endowing the stacked transformed features \mathbf{z}_i with the additive factor model above, i.e. $\mathbf{z}_{mi} \sim \mathcal{N}_{p_m}(\boldsymbol{\mu}_m + \mathbf{A}_m \boldsymbol{\eta}_i, \boldsymbol{\Gamma}_m \boldsymbol{\Gamma}_m^\top + \text{diag}(\boldsymbol{\sigma}_m^2))$, we have that $p(\boldsymbol{\eta}_i|\mathbf{z}_i)$ is pdf of a normal distribution with mean $\mathbf{A} \mathbf{z}_i$ and variance \mathbf{V} (see Proposition 1). In this case, the above integral can be solved when $g^{-1}(\cdot)$ is the identity function, as in linear regression, or the exponential function, as in regression for count data or survival analysis. On the contrary, when we are dealing with a binary regression and $g^{-1}(\cdot)$ is equal to the logit, the above integral does not have an analytical solution. However, recalling that in such case φ_i represents the probability of success, we can integrate out the latent variables and compute the expectation of the log-odds conditional on \mathbf{z}_i

$$\mathbb{E}\left[\log\left(\frac{\varphi_i}{1 - \varphi_i}\right) \middle| \mathbf{z}_i\right] = \mathbb{E}[\boldsymbol{\theta}^\top \boldsymbol{\eta}_i + \boldsymbol{\eta}_i^\top \boldsymbol{\Omega} \boldsymbol{\eta}_i | \mathbf{z}_i] = (\boldsymbol{\theta}^\top \mathbf{A}) \mathbf{z}_i + \mathbf{z}_i^\top (\mathbf{A}^\top \boldsymbol{\Omega} \mathbf{A}) \mathbf{z}_i + \text{tr}(\boldsymbol{\Omega} \mathbf{V}).$$

Appendix D Generating Realistic Loadings Matrices

In the current section, we describe an original way to generate loading matrices inducing realistic block-structured correlations. This represents a significant improvement in targeting realistic simulated data, compared to many studies in the literature. Focusing on a single loading matrix $\mathbf{\Lambda} \in \mathbb{R}^{p \times K}$ for ease of notation, Ding et al. (2022) set $\mathbf{\Lambda} = [\mathbf{I}_K, \mathbf{0}_{K \times (p-K)}]^\top$, which gives $\mathbf{\Lambda}\mathbf{\Lambda}^\top = \text{block-diag}(\{\mathbf{I}_K, \mathbf{0}_{K \times (p-K)}\})$. Samorodnitsky et al. (2024) samples independently $\Lambda_{jh} \sim \mathcal{N}(0, 1)$, so that $\mathbb{E}[(\mathbf{\Lambda}\mathbf{\Lambda}^\top)_{jj'}] = \delta_{j,j'} \cdot K$. Poworoznek et al. (2021) enforce a simple sparsity pattern in the loadings, dividing the p features into K groups and sampling $\Lambda_{jh} \sim \delta_{g(j),h} \mathcal{N}(0, v_{slab}^2) + (1 - \delta_{g(j),h}) \mathcal{N}(0, v_{spike}^2)$, for some $v_{slab}^2 \gg v_{spike}^2$ and representing by $g(j)$ the group assignment. This still gives $\mathbb{E}[(\mathbf{\Lambda}\mathbf{\Lambda}^\top)_{jj'}] = \delta_{j,j'} \cdot (v_{slab}^2 + (K-1) \cdot v_{spike}^2)$. Although the generation of a specific loading matrix entails single samples rather than expectations, the induced correlation matrices are not expected to present any meaningful structure. To overcome this issue, we further leverage the grouping of the features, allowing each group to load on multiple latent factors and centering the entries of each group around some common hyper-loading μ_g , for $g = 1, \dots, G$. To induce blocks of positive and negatively correlated features, we propose setting $\mu_g = (-1)^g \tilde{\mu}_g$, with $\tilde{\mu}_g$ sampled from a density f_+ with support on the positive real line. Our default suggestion is to set f_+ to be a beta distribution $\mathcal{Be}(5, 3)$. Conditioned on such hyper-loadings and the group assignments, we sample the loading entries independently from $\Lambda_{jh} \sim \mathcal{N}(\mu_{g(j)}/\sqrt{K}, v_o^2/K)$, resulting in $\mathbb{E}[(\mathbf{\Lambda}\mathbf{\Lambda}^\top)_{jj'}] = (-1)^{g(j)}(-1)^{g(j')} \tilde{\mu}_{g(j)} \tilde{\mu}_{g(j')} + \delta_{j,j'} v_o^2$. This naturally translates into blocks of features with correlations of alternating signs and different magnitudes. The core structure above can be complemented with further nuances, to recreate more realistic patterns. This includes group-wise sign permutation, introducing entry-wise and group-wise sparsity, and the addition of a layer of noise loadings $\mathcal{N}(0, r_{damp} v_o^2/K)$ to avoid exact zeros. In our simulation studies from Section 3, we set $v_o^2 = 0.1$ and $r_{damp} = 1e^{-2}$. Finally, view-wise sparsity can be imposed on the shared loadings of the JAFAR structure to achieve composite activity patterns in the respective component of the model. The resulting generation procedure for a view-specific loading matrix is summarized in Algorithm D1.

Algorithm D1: Generation of Realistic Loading Matrices.

```

 $\mathbf{\Lambda} = \mathbf{0}_{p \times K}$ 
for  $g = 1, \dots, G$  do
     $\tilde{\mu}_g \sim f_+$  [hyper-loadings magnitude]
     $\mu_g = (-1)^g \tilde{\mu}_g$  [signed hyper-loadings]
    for  $h = 1, \dots, K$  do
         $u_{gh} \sim \text{Bern}(\pi^{(g)})$  [group-wise sparsity]
         $s_{gh} \sim \text{Bern}(\pi^{(s)})$  [group-wise sign switch]
    for  $j = 1, \dots, p$  do
         $g(j) \sim \text{Cat}_G(\{\pi_g\}_{g=1}^G)$  [group assignment]
        for  $h = 1, \dots, K$  do
             $r_{jh} \sim \text{Bern}(\pi^{(e)})$  [entry-wise sparsity]
             $\ell_{jh}^{(1)} \sim \mathcal{N}(\mu_g/\sqrt{K}, v_o^2/K)$  [main signal]
             $\ell_{jh}^{(o)} \sim \mathcal{N}(0, r_{damp} v_o^2/K)$  [spurious signal]
             $\Lambda_{jh} = u_{g(j)h} \cdot (2s_{g(j)h} - 1) \cdot r_{jh} \cdot \ell_{jh}^{(1)} + \ell_{jh}^{(o)}$  [composite signal]
    Return  $\mathbf{\Lambda}$ 

```
